Radical ligand transfer: mechanism and reactivity governed by three-component thermodynamics

Zuzanna Wojdyla[a] and Martin Srnec[a,*]

J. Heyrovský Institute of Physical Chemistry, Czech Academy of Sciences, Prague 182 23, Czech Republic

Correspondence: martin.srnec@jh-inst.cas.cz

Table of Contents

Conformations of the (L)(TMC)Fe^{III}–OH complexes

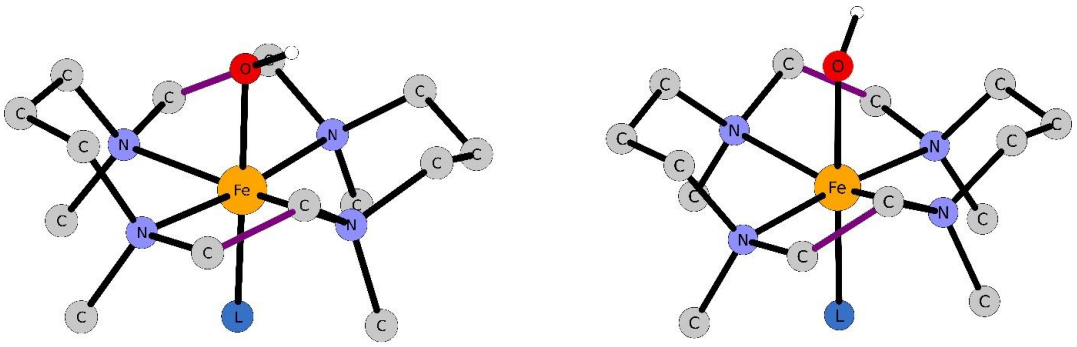

Figure S1. Crossed and parallel conformations of TMC. The crucial bonds are colored purple.

The thermodynamic half-reaction cycles for concerted ion-electron transfers between the $Fe^{III}OH$ ($OH^{\bullet}$ donor) and substrate radical ($Sub^{\bullet}$, $OH^{\bullet}$ donor)

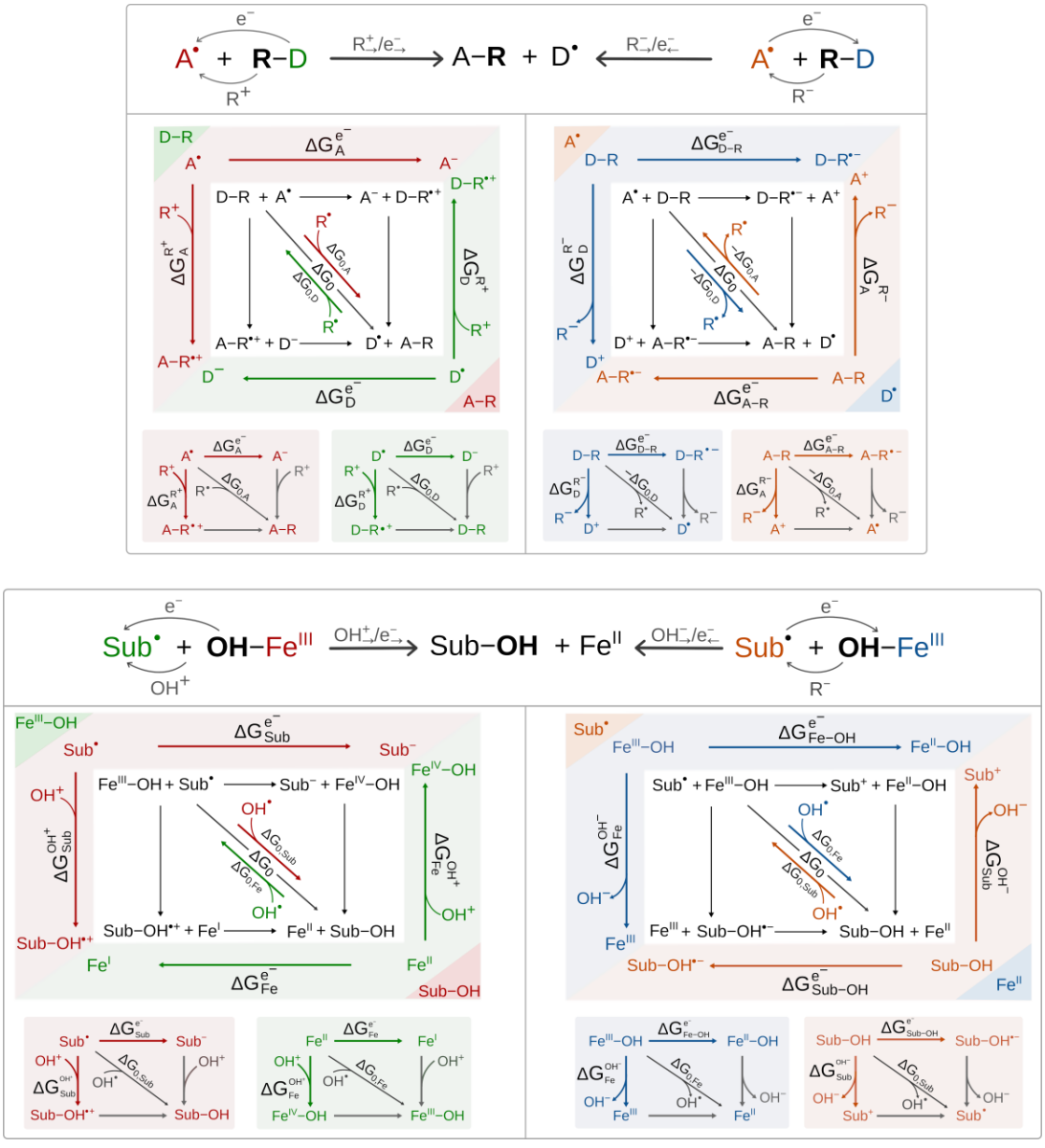

Figure S2. Top panel: two mechanistic scenarios for radical ligand transfers between the $R^{\bullet}$ donor (D–R) and acceptor ($A^{\bullet}$): one involving concerted and co-directional transfer of R^{+} and electron denoted as $R^{+}_{\rightarrow}/e^{-}_{\rightarrow}$ transfer, and one with concerted contra-directional transfer of R^{-} and electron denoted as $R^{-}_{\rightarrow}/e^{-}_{\leftarrow}$. The full reaction thermodynamic cycles associated with the two transfer mechanisms are depicted together with their constituent blocks – half-reaction thermodynamic cycles. For each half-reaction thermodynamic cycle, three key free energy quantities are shown. Bottom panel: two mechanistic scenarios for OH transfer between the FeIIIOH and the substrate.

Thermodynamic and reactivity data for the sets of model (L)(TMC)Fe^{III}-OH complexes

Table S1. Thermodynamic data for the set of axially-substituted model (L)(TMC)Fe^{III}–OH complexes ('parallel' set) for the OH^- and OH^+ cycles. The values were obtained at the B3LYP(D3)/def2-SVP level, with implicit CPCM solvation in MeCN at 298 K. All energies are given in kcal mol^{-1}.

	OH^- cycle					OH+ cycle				
ligand	ΔG^{e^-} (D-R)	ΔG^{OH^-} (D-R)	ω^{OH^-}	μ^{OH^-}	ΔG_0 (half cycle)	ΔG^{e^-} (D$^\bullet$)	ΔG^{OH^+} (D$^\bullet$)	ω^{OH^+}	μ^{OH^+}	ΔG_0 (half cycle)
Br	-98.26	85.20	-129.72	-9.23	-45.63	-41.83	-170.16	91.35	-150.51	-319.39
Cl	-95.89	85.10	-127.98	-7.63	-43.92	-37.23	-171.67	95.06	-147.71	-321.10
CN	-98.07	90.93	-133.64	-5.05	-44.78	-48.88	-176.00	89.89	-159.01	-320.24
NC	-98.92	91.39	-134.57	-5.32	-42.67	-44.39	-174.38	91.92	-154.69	-322.35
NCS	-97.78	84.55	-128.93	-9.36	-42.15	-45.39	-177.31	93.29	-157.47	-322.87
OH	-83.62	75.10	-112.23	-6.03	-38.29	-20.36	-192.42	121.67	-150.46	-326.73
NH_2	-79.51	69.62	-105.45	-6.99	-38.53	-19.41	-198.81	126.85	-154.31	-326.48
N_3	-94.13	79.96	-123.10	-10.02	-42.04	-38.58	-179.08	99.35	-153.91	-322.98
$OOCCF_3$	-98.96	90.55	-134.00	-5.94	-42.56	-41.88	-169.78	90.44	-149.66	-322.45
thiolate	-90.61	77.91	-119.17	-8.98	-39.80	-37.20	-189.30	107.55	-160.15	-325.22
carboxylate tethered	-95.90	92.25	-133.04	-2.58	-37.61	-41.27	-184.71	101.42	-159.79	-327.41
carboxylate untethered	-94.62	83.75	-126.13	-7.69	-43.84	-35.46	-173.23	97.42	-147.57	-321.18
	ΔG^{e^-} (A-R)	ΔG^{OH^-} (A-R)	ω^{OH^-}	μ^{OH^-}	ΔG_0 (half cycle)	ΔG^{e^-} (A$^\bullet$)	ΔG^{OH^+} (A$^\bullet$)	ω^{OH^+}	μ^{OH^+}	ΔG_0 (half cycle)
CHD$^\bullet$	-106.01	84.93	-71.74	48.37	-21.08	-147.75	-196.19	100.63	-176.83	-343.94
2F-CHD$^\bullet$	-138.11	115.33	-109.64	53.46	-22.78	-165.33	-176.91	64.72	-185.46	-342.24

Table S2. Reactivity data for the TMC/CHD$^{\bullet}$ set (‘**parallel’,** antiferromagnetically coupled reactants). The values were obtained at the B3LYP(D3)/def2-SVP level, with implicit CPCM solvation in MeCN at 298 K. All energies are given in kcal mol^{-1}.

			OH$^-$ w/CHD$^{\bullet}$				OH$^+$ w/CHD$^{\bullet}$			
ligand	ΔG_0	$\Delta G^{\neq}$	η_{OH^-}	σ_{OH^-}	$\Delta G^{\neq}_{off-diagonal}$	$\Delta G^{\neq}_{thermo,OH^-}$	η_{OH^+}	σ_{OH^+}	$\Delta G^{\neq}_{off-diagonal}$	$\Delta G^{\neq}_{thermo,OH^+}$
Br	-24.55	6.26	-57.98	-57.61	**-0.09**	-12.37	-9.28	26.32	**4.26**	-8.02
Cl	-22.84	6.61	-56.24	-56.00	**-0.06**	-11.48	-5.57	29.12	**5.89**	-5.54
CN	-23.70	5.50	-61.91	-53.42	**-2.12**	-13.97	-10.74	17.81	**1.77**	-10.08
NC	-21.59	5.51	-62.83	-53.69	**-2.28**	-13.08	-8.71	22.13	**3.36**	-7.44
NCS	-21.07	6.18	-57.19	-57.73	**0.14**	-10.40	-7.35	19.36	**3.00**	-7.53
OH	-17.22	14.12	-40.49	-54.40	**3.48**	-5.13	21.04	26.37	**1.33**	-7.27
NH2	-17.46	----	-33.72	-55.37	**5.41**	-3.32	26.22	22.52	**-0.92**	-9.65
N3	-20.97	8.96	-51.36	-58.39	**1.76**	-8.73	-1.28	22.92	**5.41**	-5.07
OOCCF3	-21.49	5.45	-62.26	-54.31	**-1.99**	-12.73	-10.19	27.16	**4.24**	-6.50
thiolate	-18.72	---	-47.43	-57.35	**2.48**	-6.88	6.92	16.67	**2.44**	-6.92
carboxylate tethered	-16.53	7.10	-61.30	-50.95	**-2.59**	-10.85	0.79	17.04	**4.06**	-4.20
carboxylate untethered	-22.76	8.29	-54.39	-56.06	**0.42**	-10.96	-2.11	28.54	**6.61**	-4.77

Table S3. Reactivity data for the TMC/2F-CHD• set (‘**parallel**’, antiferromagnetically coupled reactants). The values were obtained at the B3LYP(D3)/def2-SVP level, with implicit CPCM solvation in MeCN at 298 K. All energies are given in kcal mol^{-1}.

			OH^- w/ 2F-CHD•				OH^+ w/2F-CHD•			
ligand	ΔG_0	$\Delta G^{\neq}$	η_{OH^-}	σ_{OH^-}	$\Delta G^{\neq}_{off-diagonal}$	$\Delta G^{\neq}_{thermo,OH^-}$	η_{OH^+}	σ_{OH^+}	$\Delta G^{\neq}_{off-diagonal}$	$\Delta G^{\neq}_{thermo,OH^+}$
Br	-22.85	15.63	-20.08	-62.69	**10.65**	-0.77	-26.63	-34.95	**2.08**	-9.34
Cl	-21.14	14.99	-18.34	-61.08	**10.69**	0.12	-30.34	-37.75	**1.85**	-8.72
CN	-21.99	15.13	-24.00	-58.50	**8.62**	-2.37	-25.17	-26.45	**0.32**	-10.68
NC	-19.89	14.81	-24.93	-58.78	**8.46**	-1.48	-27.20	-30.77	**0.89**	-9.05
NCS	-19.37	15.93	-19.29	-62.81	**10.88**	1.20	-28.57	-27.99	**-0.14**	-9.83
OH	-15.51	18.19	-2.59	-59.48	**14.22**	6.47	-56.95	-35.00	**-5.49**	-13.24
NH2	-15.75	19.37	4.19	-60.45	**14.07**	6.19	-62.13	-31.15	**-7.74**	-15.62
N3	-19.26	16.20	-13.46	-63.47	**12.50**	2.87	-34.63	-31.55	**-0.77**	-10.40
OOCCF3	-19.78	15.12	-24.36	-59.40	**8.76**	-1.13	-25.72	-35.80	**2.52**	-7.37
thiolate	-17.02	17.01	-9.53	-62.43	**13.23**	4.72	-42.83	-25.31	**-4.38**	-12.89
carboxylate tethered	-14.82	14.97	-23.40	-56.04	**8.16**	0.75	-36.70	-25.67	**-2.76**	-10.17
carboxylate untethered	-21.05	16.98	-16.49	-61.14	**11.16**	0.64	-33.80	-37.17	**0.84**	-9.69

Table S4. Thermodynamic data for the set of axially-substituted model (L)(TMC)Fe^{III}–OH complexes ('**crossed**' set) for the OH^- and OH^+ cycles. The values were obtained at the B3LYP(D3)/def2-SVP level, with implicit CPCM solvation in MeCN at 298 K. All energies are given in kcal mol^{-1}.

	OH^- cycle					OH^+ cycle				
ligand	ΔG^{e^-} (D-R)	ΔG^{OH^-} (D-R)	ω^{OH^-}	μ^{OH^-}	ΔG_0 (half cycle)	ΔG^{e^-} (D•)	ΔG^{OH^+} (D•)	ω^{OH^+}	μ^{OH^+}	ΔG_0 (half cycle)
Br	-98.87	79.90	-126.41	-13.41	-49.77	-41.99	-164.92	86.92	-146.31	-306.14
Cl	-96.49	81.24	-125.68	-10.79	-47.71	-36.64	-169.00	93.59	-145.41	-317.31
CN	-97.64	86.25	-130.03	-8.05	-48.33	-47.87	-171.83	87.65	-155.34	-316.69
NC	-98.48	86.16	-130.56	-8.71	-47.33	-43.74	-169.49	88.92	-150.77	-317.69
NCS	-98.18	81.53	-127.08	-11.77	-44.67	-45.55	-175.66	92.00	-156.42	-320.35
OH	-83.61	72.23	-110.19	-8.05	-41.46	-21.34	-190.19	119.40	-149.58	-323.56
NH_2	-79.44	66.00	-102.84	-9.50	-41.50	-18.69	-195.08	124.73	-151.16	-323.52
N_3	-94.16	75.70	-120.11	-13.05	-43.31	-39.77	-178.41	98.04	-154.28	-321.71
$OOCCF_3$	-99.70	84.95	-130.57	-10.42	-46.97	-40.81	-167.29	89.43	-147.15	-318.05
thiolate	-90.40	76.19	-115.63	-12.21	-43.79	-37.54	-186.20	105.12	-158.21	-321.23
carboxylate tethered	-95.29	89.09	-130.38	-4.38	-40.60	-38.13	-181.96	101.70	-155.63	-324.42
carboxylate untethered	-94.72	79.25	-123.02	-10.94	-46.04	-35.46	-173.23	97.42	-147.57	-318.98

Table S5. Reactivity data for the TMC/CHD$^{\bullet}$ set ('**crossed**', antiferromagnetically coupled reactants). The values were obtained at the B3LYP(D3)/def2-SVP level. with implicit CPCM solvation in MeCN at 298 K. All energies are given in kcal mol^{-1}.

			OH^- w/CHD$^{\bullet}$				OH^+ w/CHD$^{\bullet}$			
ligand	ΔG_0	$\Delta G^{\neq}$	η_{OH^-}	σ_{OH^-}	$\Delta G^{\neq}_{off-diagonal}$	$\Delta G^{\neq}_{thermo,OH^-}$	η_{OH^+}	σ_{OH^+}	$\Delta G^{\neq}_{off-diagonal}$	$\Delta G^{\neq}_{thermo,OH^+}$
Br	-28.69	5.53	-54.67	-61.78	1.78	-12.57	-13.71	30.52	4.20	-10.14
Cl	-26.64	6.70	-53.94	-59.16	1.31	-12.01	-7.04	31.42	6.10	-7.22
CN	-27.25	6.33	-58.29	-56.43	-0.47	-14.09	-12.98	21.48	2.13	-11.50
NC	-26.25	6.42	-58.82	-57.08	-0.43	-13.56	-11.71	26.06	3.59	-9.54
NCS	-23.60	6.19	-55.34	-60.15	1.20	-10.60	-8.63	20.41	2.94	-8.85
OH	-20.39	14.36	-38.46	-56.42	4.49	-5.70	18.76	27.25	2.12	-8.07
NH_2	-20.42	---	-31.10	-57.88	6.69	-3.52	24.09	25.67	0.39	-9.82
N_3	-22.23	8.83	-48.37	-61.42	3.26	-7.85	-2.60	22.55	4.99	-6.13
$OOCCF_3$	-25.89	5.08	-58.83	-58.80	-0.01	-12.95	-11.20	29.68	4.62	-8.33
thiolate	-22.71	---	-43.89	-60.59	4.17	-7.18	4.48	18.62	4.48	18.62
carboxylate tethered	-19.52	7.55	-58.64	-52.76	-1.47	-11.23	1.07	21.20	5.03	-4.73
carboxylate untethered	-24.96	8.10	-51.28	-59.31	2.01	-10.47	-3.21	29.26	6.51	-5.97

Table S6. Reactivity data for the TMC/2F-CHD• set (‘**crossed**’, antiferromagnetically coupled reactants). The values were obtained at the B3LYP(D3)/def2-SVP level. with implicit CPCM solvation in MeCN at 298 K. All energies are given in kcal mol^{-1}.

			OH$^-$ w/2F-CHD•				OH$^+$ w/2F-CHD•			
ligand	ΔG_0	$\Delta G^{\neq}$	η_{OH^-}	σ_{OH^-}	$\Delta G^{\neq}_{off-diagonal}$	$\Delta G^{\neq}_{thermo,OH^-}$	η_{OH^+}	σ_{OH^+}	$\Delta G^{\neq}_{off-diagonal}$	$\Delta G^{\neq}_{thermo,OH^+}$
Br	-26.99	14.84	-16.77	-66.86	12.52	-0.97	-22.20	-39.15	4.24	-9.26
Cl	-24.93	16.09	-16.04	-64.24	12.05	-0.41	-28.87	-40.05	2.80	-9.67
CN	-25.55	14.70	-20.39	-61.51	10.28	-2.49	-22.93	-30.12	1.80	-10.98
NC	-24.54	15.13	-20.92	-62.17	10.31	-1.96	-24.20	-34.69	2.62	-9.65
NCS	-21.89	14.69	-17.44	-65.23	11.95	1.00	-27.28	-29.04	0.44	-10.50
OH	-18.68	19.70	-0.55	-61.50	15.24	5.90	-54.67	-35.88	-4.70	-14.04
NH_2	-18.71	21.46	6.80	-62.96	14.04	4.68	-60.01	-34.30	-6.43	-15.78
N_3	-20.52	16.38	-10.47	-66.51	14.01	3.75	-33.31	-31.18	-0.53	-10.79
$OOCCF_3$	-24.18	14.41	-20.93	-63.88	10.74	-1.35	-24.71	-38.31	3.40	-8.69
thiolate	-21.01	16.25	-5.99	-65.67	14.92	4.42	-40.40	-27.25	-3.29	-13.79
carboxylate tethered	-17.82	15.47	-20.74	-57.84	9.27	0.37	-36.98	-29.83	-1.79	-10.70
carboxylate untethered	-23.25	16.43	-13.37	-64.40	12.76	1.13	-32.70	-37.89	1.30	-10.33

Table S7. Reactivity data for the TMC/CHD$^{\bullet}$ set ('**parallel**', ferromagnetically coupled reactants). The values were obtained at the B3LYP(D3)/def2-SVP level, with implicit CPCM solvation in MeCN at 298 K. All energies are given in kcal mol^{-1}.

			OH^- w/CHD$^{\bullet}$				OH^+ w/CHD$^{\bullet}$			
ligand	ΔG_0	$\Delta G^{\neq}$	η_{OH^-}	σ_{OH^-}	$\Delta G^{\neq}_{off-diagonal}$	$\Delta G^{\neq}_{thermo,OH^-}$	η_{OH^+}	σ_{OH^+}	$\Delta G^{\neq}_{off-diagonal}$	$\Delta G^{\neq}_{thermo,OH^+}$
Br	-35.02	-1.71	-57.98	-57.61	**-0.09**	-17.92	-9.28	26.32	**4.26**	-13.57
Cl	-32.83	-0.29	-56.24	-56.00	**-0.06**	-16.47	-5.57	29.12	**5.89**	-10.53
CN	-25.54	3.74	-61.91	-53.42	**-2.12**	-14.89	-10.74	17.81	**1.77**	-11.00
NC	-27.64	0.64	-62.83	-53.69	**-2.28**	-16.11	-8.71	22.13	**3.36**	-10.46
NCS	-28.56	0.58	-57.19	-57.73	**0.14**	-14.14	-7.35	19.36	**3.00**	-11.27
OH	-20.04	8.97	-40.49	-54.40	**3.48**	-6.54	21.04	26.37	**1.33**	-8.69
NH2	-20.44	12.59	-33.72	-55.37	**5.41**	-4.81	26.22	22.52	**-0.92**	-11.14
N3	-29.89	0.74	-51.36	-58.39	**1.76**	-13.19	-1.28	22.92	**5.41**	-9.53
OOCCF3	-30.64	-0.88	-62.26	-54.31	**-1.99**	-17.31	-10.19	27.16	**4.24**	-11.08
thiolate	-20.93	7.56	-47.43	-57.35	**2.48**	-7.98	6.92	16.67	**2.44**	-8.02
carboxylate tethered	-21.91	1.95	-61.30	-50.95	**-2.59**	-13.54	0.79	17.04	**4.06**	-6.89
carboxylate untethered	-30.96	0.52	-54.39	-56.06	**0.42**	-15.06	-2.11	28.54	**6.61**	-8.87

Table S8. Reactivity data for the TMC/2F-CHD• set (‘**parallel**’, ferromagnetically coupled reactants). The values were obtained at the B3LYP(D3)/def2-SVP level, with implicit CPCM solvation in MeCN at 298 K. All energies are given in kcal mol^{-1}.

			OH^- w/ 2F-CHD•				OH^+ w/2F-CHD•			
ligand	ΔG_0	$\Delta G^{\neq}$	η_{OH^-}	σ_{OH^-}	$\Delta G^{\neq}_{off-diagonal}$	$\Delta G^{\neq}_{thermo,OH^-}$	η_{OH^+}	σ_{OH^+}	$\Delta G^{\neq}_{off-diagonal}$	$\Delta G^{\neq}_{thermo,OH^+}$
Br	-33.32	8.40	-20.08	-62.69	**10.65**	-6.32	-26.63	-34.95	**2.08**	-14.59
Cl	-31.12	7.83	-18.34	-61.08	**10.69**	-4.87	-30.34	-37.75	**1.85**	-13.71
CN	-23.84	11.58	-24.00	-58.50	**8.62**	-3.29	-25.17	-26.45	**0.32**	-11.60
NC	-25.94	8.42	-24.93	-58.78	**8.46**	-4.51	-27.20	-30.77	**0.89**	-12.08
NCS	-26.85	8.74	-19.29	-62.81	**10.88**	-2.54	-28.57	-27.99	**-0.14**	-13.57
OH	-18.33	14.62	-2.59	-59.48	**14.22**	05.06	-56.95	-35.00	**-5.49**	-14.65
NH2	-18.74	16.77	4.19	-60.45	**14.07**	4.70	-62.13	-31.15	**-7.74**	-17.11
N3	-28.18	11.57	-13.46	-63.47	**12.50**	-1.59	-34.63	-31.55	**-0.77**	-14.86
OOCCF3	-28.93	7.29	-24.36	-59.40	**8.76**	-5.71	-25.72	-35.80	**2.52**	-11.95
thiolate	-19.22	13.91	-9.53	-62.43	**13.23**	3.62	-42.83	-25.31	**-4.38**	-13.99
carboxylate tethered	-20.20	11.03	-23.40	-56.04	**8.16**	-1.94	-36.70	-25.67	**-2.76**	-12.86
carboxylate untethered	-29.25	9.80	-16.49	-61.14	**11.16**	-3.46	-33.80	-37.17	**0.84**	-13.78

Table S9. Reactivity data for the TMC/CHD• set (‘**crossed**’, ferromagnetically coupled reactants). The values were obtained at the B3LYP(D3)/def2-SVP level. with implicit CPCM solvation in MeCN at 298 K. All energies are given in kcal mol^{-1}.

			OH^- w/CHD•				OH^+ w/CHD•			
ligand	ΔG_0	$\Delta G^{\neq}$	η_{OH^-}	σ_{OH^-}	$\Delta G^{\neq}_{off-diagonal}$	$\Delta G^{\neq}_{thermo,OH^-}$	η_{OH^+}	σ_{OH^+}	$\Delta G^{\neq}_{off-diagonal}$	$\Delta G^{\neq}_{thermo,OH^+}$
Br	-37.80	-0.97	-54.67	-61.78	**1.78**	-17.13	-13.71	30.52	**4.20**	-10.14
Cl	-35.26	-0.50	-53.94	-59.16	**1.31**	-16.32	-7.04	31.42	**6.10**	-7.22
CN	-28.95	4.16	-58.29	-56.43	**-0.47**	-14.94	-12.98	21.48	**2.13**	-11.50
NC	-32.75	-0.30	-58.82	-57.08	**-0.43**	-16.81	-11.71	26.06	**3.59**	-9.54
NCS	-30.47	0.16	-55.34	-60.15	**1.20**	-14.03	-8.63	20.41	**2.94**	-8.85
OH	-22.64	9.81	-38.46	-56.42	**4.49**	-6.83	18.76	27.25	**2.12**	-8.07
NH_2	-23.32	12.80	-31.10	-57.88	**6.69**	-4.97	24.09	25.67	**0.39**	-9.82
N_3	-29.86	0.98	-48.37	-61.42	**3.26**	-11.67	-2.60	22.55	**4.99**	-6.13
$OOCCF_3$	-34.29	-1.75	-58.83	-58.80	**-0.01**	-17.15	-11.20	29.68	**4.62**	-8.33
thiolate	-24.68	8.08	-43.89	-60.59	**4.17**	-8.16	4.48	18.62	**4.48**	-8.80
carboxylate tethered	-26.65	0.97	-58.64	-52.76	**-1.47**	-14.80	1.07	21.20	**5.03**	-4.73
carboxylate untethered	-32.81	0.34	-51.28	-59.31	**2.01**	-14.40	-3.21	29.26	**6.51**	-5.97

Table S10. Reactivity data for the TMC/2F-CHD• set ('**crossed**', ferromagnetically coupled reactants). The values were obtained at the B3LYP(D3)/def2-SVP level. with implicit CPCM solvation in MeCN at 298 K. All energies are given in kcal mol^{-1}.

			OH^- w/CHD•				OH^+ w/CHD•			
ligand	ΔG_0	$\Delta G^{\neq}$	η_{OH^-}	σ_{OH^-}	$\Delta G^{\neq}_{off-diagonal}$	$\Delta G^{\neq}_{thermo,OH^-}$	η_{OH^+}	σ_{OH^+}	$\Delta G^{\neq}_{off-diagonal}$	$\Delta G^{\neq}_{thermo,OH^+}$
Br	-36.10	6.87	-16.77	-66.86	**12.52**	-5.53	-22.20	-39.15	**4.24**	-13.81
Cl	-33.55	8.40	-16.04	-64.24	**12.05**	-4.73	-28.87	-40.05	**2.80**	-13.98
CN	-27.25	-1.9	-20.39	-61.51	**10.28**	-3.34	-22.93	-30.12	**1.80**	-11.83
NC	-31.05	8.79	-20.92	-62.17	**10.31**	-5.21	-24.20	-34.69	**2.62**	-12.90
NCS	-28.76	8.74	-17.44	-65.23	**11.95**	-2.43	-27.28	-29.04	**0.44**	-13.94
OH	-20.93	16.19	-0.55	-61.50	**15.24**	4.77	-54.67	-35.88	**-4.70**	-15.16
NH_2	-21.62	17.11	6.80	-62.96	**14.04**	3.23	-60.01	-34.30	**-6.43**	-17.23
N_3	-28.15	9.41	-10.47	-66.51	**14.01**	-0.07	-33.31	-31.18	**-0.53**	-14.61
$OOCCF_3$	-32.58	6.21	-20.93	-63.88	**10.74**	-5.55	-24.71	-38.31	**3.40**	-12.89
thiolate	-22.97	13.46	-5.99	-65.67	**14.92**	3.43	-40.40	-27.25	**-3.29**	-14.77
carboxylate tethered	-24.94	10.16	-20.74	-57.84	**9.27**	-3.20	-36.98	-29.83	**-1.79**	-14.26
carboxylate untethered	-31.11	9.43	-13.37	-64.40	**12.76**	-2.80	-32.70	-37.89	**1.30**	-14.26

Application of the thermodynamic model to predict ΔG‡ of the hydroxyl transfer reactions for the 'parallel' and 'crossed' sets of reactions; with antiferro- and ferromagnetically coupled reactants

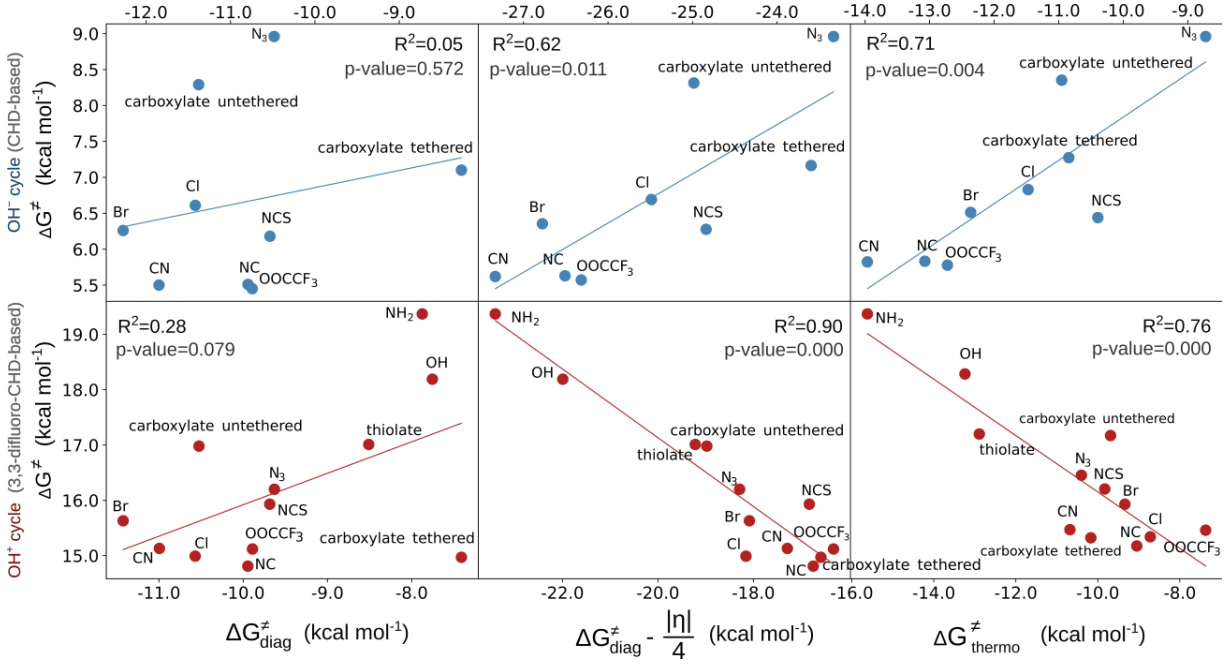

Figure S3. Three-component thermodynamics model applied to the '**parallel**' set of reactions (**antiferromagnetically** coupled reactants); $\Delta G^{\neq}$ vs: linear free energy relationship LFER (left); LFER with the effect of asynchronicity (middle) for the 'parallel' set of reactions (antiferromagnetically coupled reactants); LFER together with the complete off-diagonal term (right) for the OH^- (top) and OH^+ (bottom) set. The quality of correlations is assessed by the squared Pearson's coefficient (R^2) and p-value.

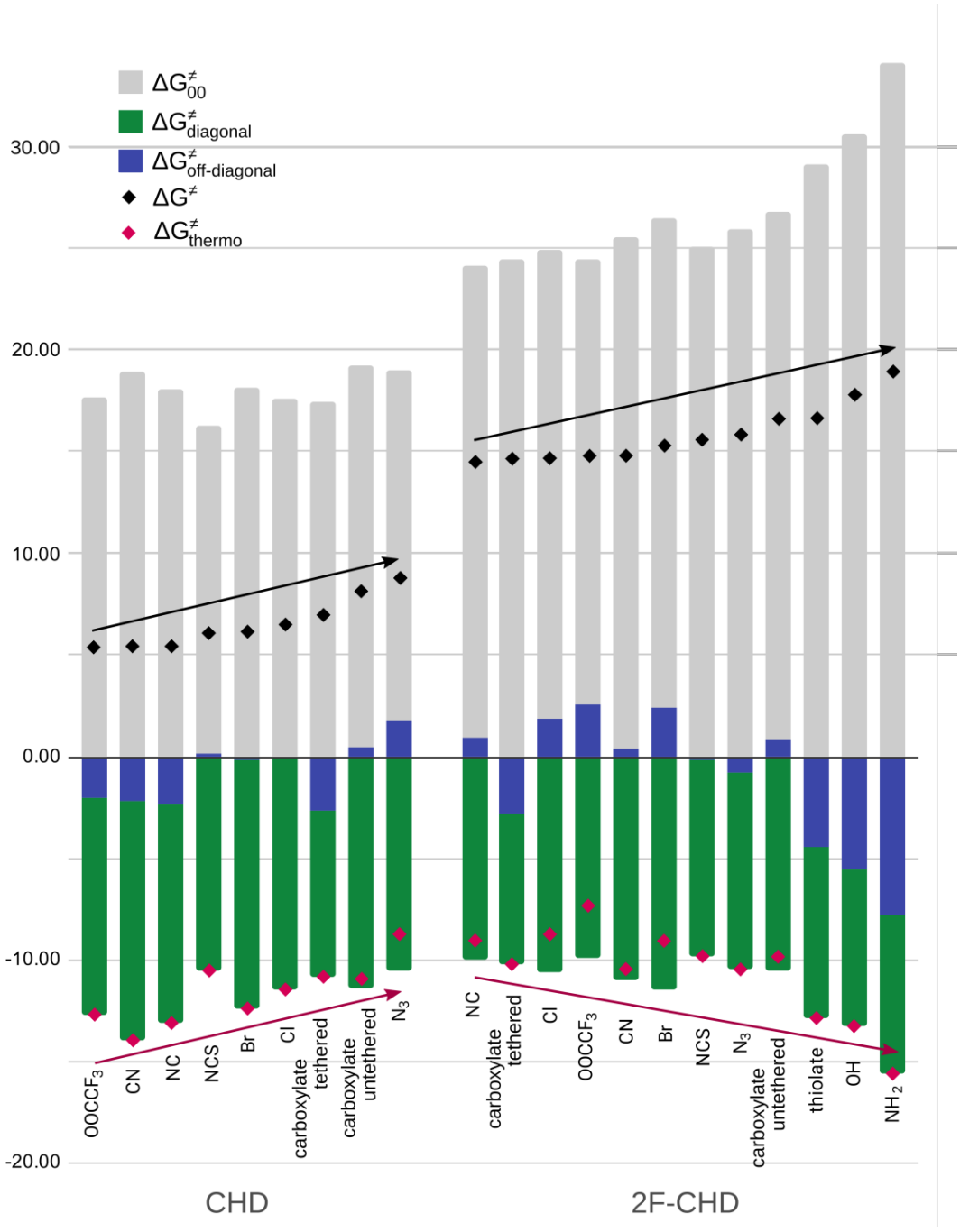

Figure S4. Decomposition of the barriers for the the '**parallel**' set of reactions (**antiferromagnetically** coupled reactants) into the non-thermodynamic and thermodynamic (diagonal and off-diagonal) components.

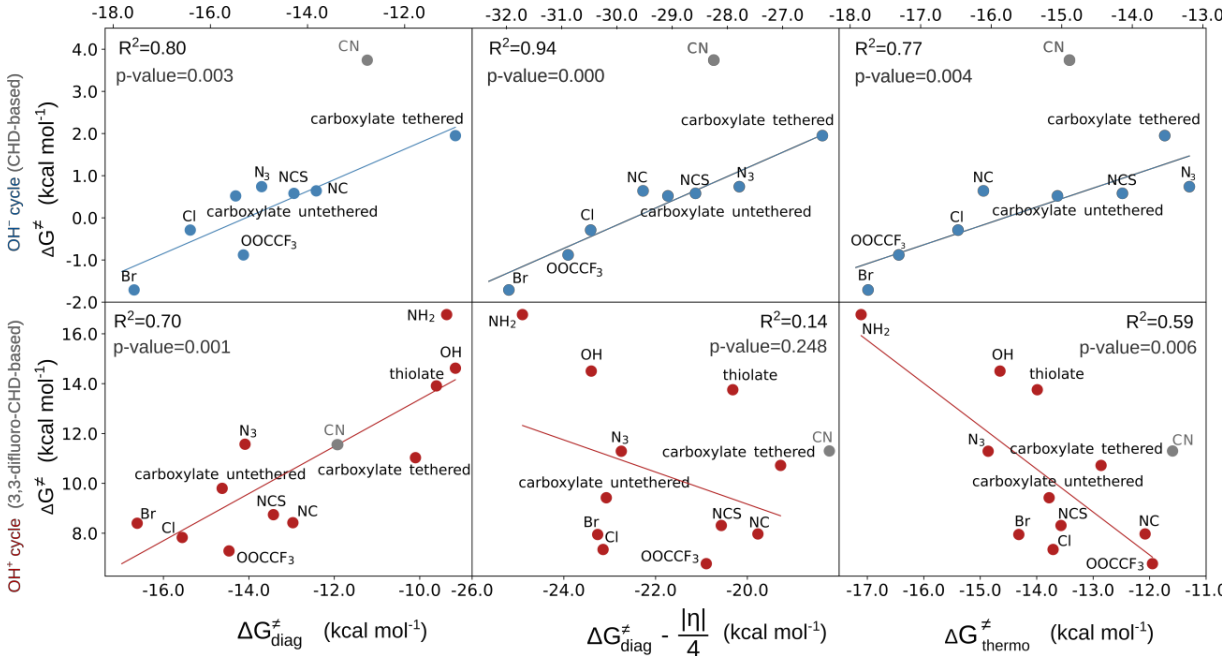

Figure S5. Three-component thermodynamics model applied to the '**parallel**' set of reactions (**ferromagnetically** coupled reactants); $\Delta G^{\neq}$ vs: linear free energy relationship LFER (left); LFER with the effect of asynchronicity (middle); LFER together with the complete off-diagonal term (right) for the OH^- (top) and OH^+ (bottom) set. The quality of correlations is assessed by the squared Pearson's coefficient (R^2) and p-value. The CN-ligated system (shown in grey) was omitted from the correlation as the barrier for OH rebound is elevated due to mismatch between the optimal geometry of the CN-(TMC)Fe^{III}–OH complex and the geometry of the complex in the TS structure.

Table S11. Performance of the model in the investigated 'parallel' sets

X axis	slope	intercept	R^2	p-value
OH^- set (antiferromagnetic)				
$\Delta G^{\neq}_{diagonal}$	0.24	9.25	0.05	0.572
$\Delta G^{\neq}_{diagonal} - \frac{\lvert\eta\rvert}{4}$	0.71	24.72	0.62	0.011
$\Delta G^{\neq}_{thermo}$	0.66	14.37	0.71	0.004
OH^+ set (antiferromagnetic)				
$\Delta G^{\neq}_{diagonal}$	0.57	21.61	0.28	0.079
$\Delta G^{\neq}_{diagonal} - \frac{\lvert\eta\rvert}{4}$	-0.62	4.70	0.90	0.000
$\Delta G^{\neq}_{thermo}$	-0.55	10.33	0.76	0.000
OH^- set (ferromagnetic)				
$\Delta G^{\neq}_{diagonal}$	0.50	7.61	0.80	0.003
$\Delta G^{\neq}_{diagonal} - \frac{\lvert\eta\rvert}{4}$	0.58	17.10	0.94	0.000
$\Delta G^{\neq}_{thermo}$	0.56	8.85	0.77	0.004
OH^+ set (ferromagnetic)				
$\Delta G^{\neq}_{diagonal}$	0.97	23.09	0.70	0.001
$\Delta G^{\neq}_{diagonal} - \frac{\lvert\eta\rvert}{4}$	-0.65	-3.51	0.14	0.249
$\Delta G^{\neq}_{thermo}$	-1.69	-12.78	0.59	0.006

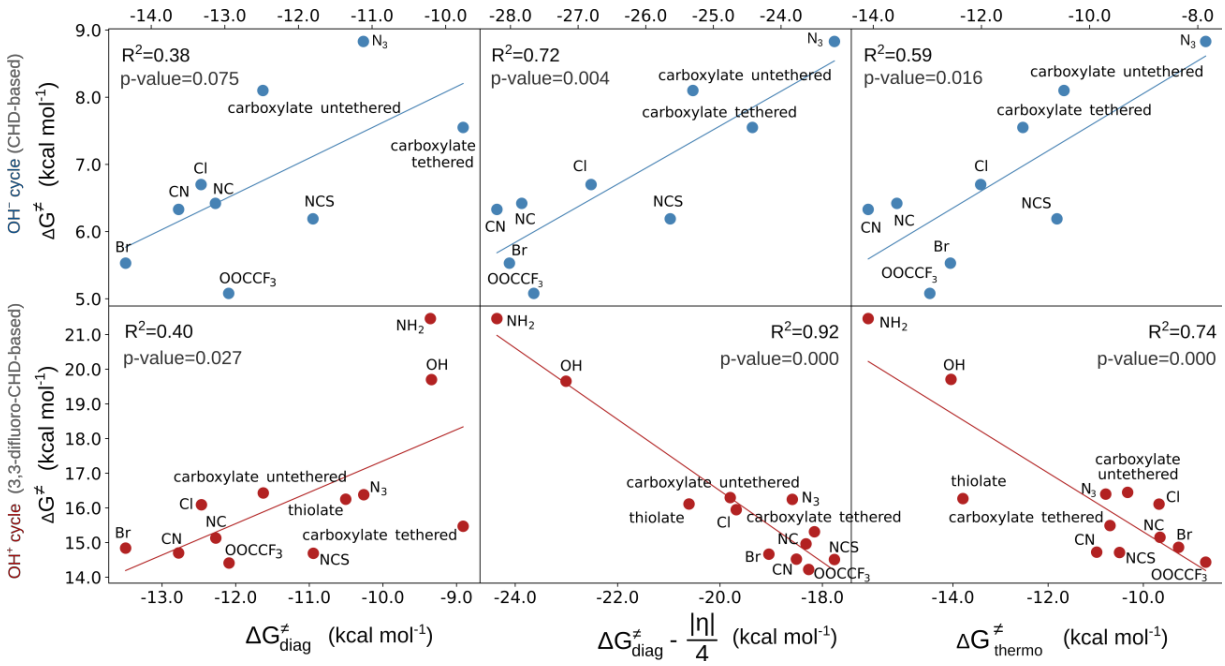

Figure S6. Three-component thermodynamics model applied to the '**crossed**' set of reactions, **antiferromagnetic** variant; $\Delta G^{\neq}$ vs: linear free energy relationship LFER (left); LFER with the effect of asynchronicity (middle); LFER together with the complete off-diagonal term (right) for the OH^- (top) and OH^+ (bottom) set. The quality of correlations is assessed by the squared Pearson's coefficient (R^2) and p-value.

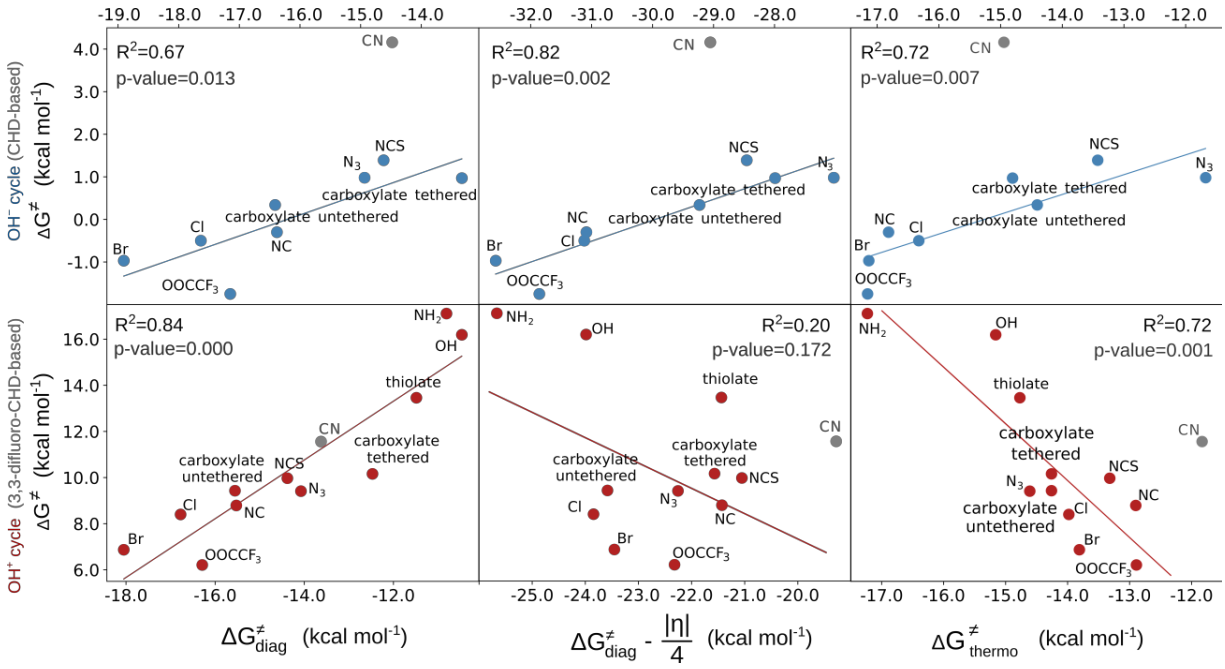

Figure S7. Three-component thermodynamics model applied to the '**crossed**' set of reactions (**ferromagnetically** coupled reactants); $\Delta G^{\neq}$ vs: linear free energy relationship LFER (left); LFER with the effect of asynchronicity (middle); LFER together with the complete off-diagonal term (right) for the OH^- (top) and OH^+ (bottom) set. The quality of correlations is assessed by the squared Pearson's coefficient (R^2) and p-value. The CN-ligated system (shown in grey) was omitted from the correlation as the barrier for rebound is elevated due to mismatch between the optimal geometry of the CN-(TMC)Fe^{III}–OH complex and the geometry of the complex in the TS structure.

Table S12. Performance of the model in the investigated 'crossed' sets

X axis	slope	intercept	R^2	p-value
OH^- set (antiferromagnetic)				
$\Delta G^{\neq}_{diagonal}$	0.53	13.39	0.38	0.075
$\Delta G^{\neq}_{diagonal} - \frac{\lvert\eta\rvert}{4}$	0.57	21.83	0.72	0.004
$\Delta G^{\neq}_{thermo}$	0.48	12.41	0.59	0.016
OH+ set (antiferromagnetic)				
$\Delta G^{\neq}_{diagonal}$	0.90	26.39	0.40	0.028
$\Delta G^{\neq}_{diagonal} - \frac{\lvert\eta\rvert}{4}$	-1.00	-3.43	0.92	0.000
$\Delta G^{\neq}_{thermo}$	-0.85	6.75	0.74	0.000
OH^- set (ferromagnetic)				
$\Delta G^{\neq}_{diagonal}$	0.49	8.00	0.67	0.013
$\Delta G^{\neq}_{diagonal} - \frac{\lvert\eta\rvert}{4}$	0.49	14.70	0.82	0.002
$\Delta G^{\neq}_{thermo}$	0.46	7.09	0.72	0.007
OH+ set (ferromagnetic)				
$\Delta G^{\neq}_{diagonal}$	1.27	28.59	0.84	0.000
$\Delta G^{\neq}_{diagonal} - \frac{\lvert\eta\rvert}{4}$	-1.10	-14.64	0.20	0.172
$\Delta G^{\neq}_{thermo}$	-2.47	-24.75	0.72	0.001

Performance of the three-component model based on the higher off-diagonal term

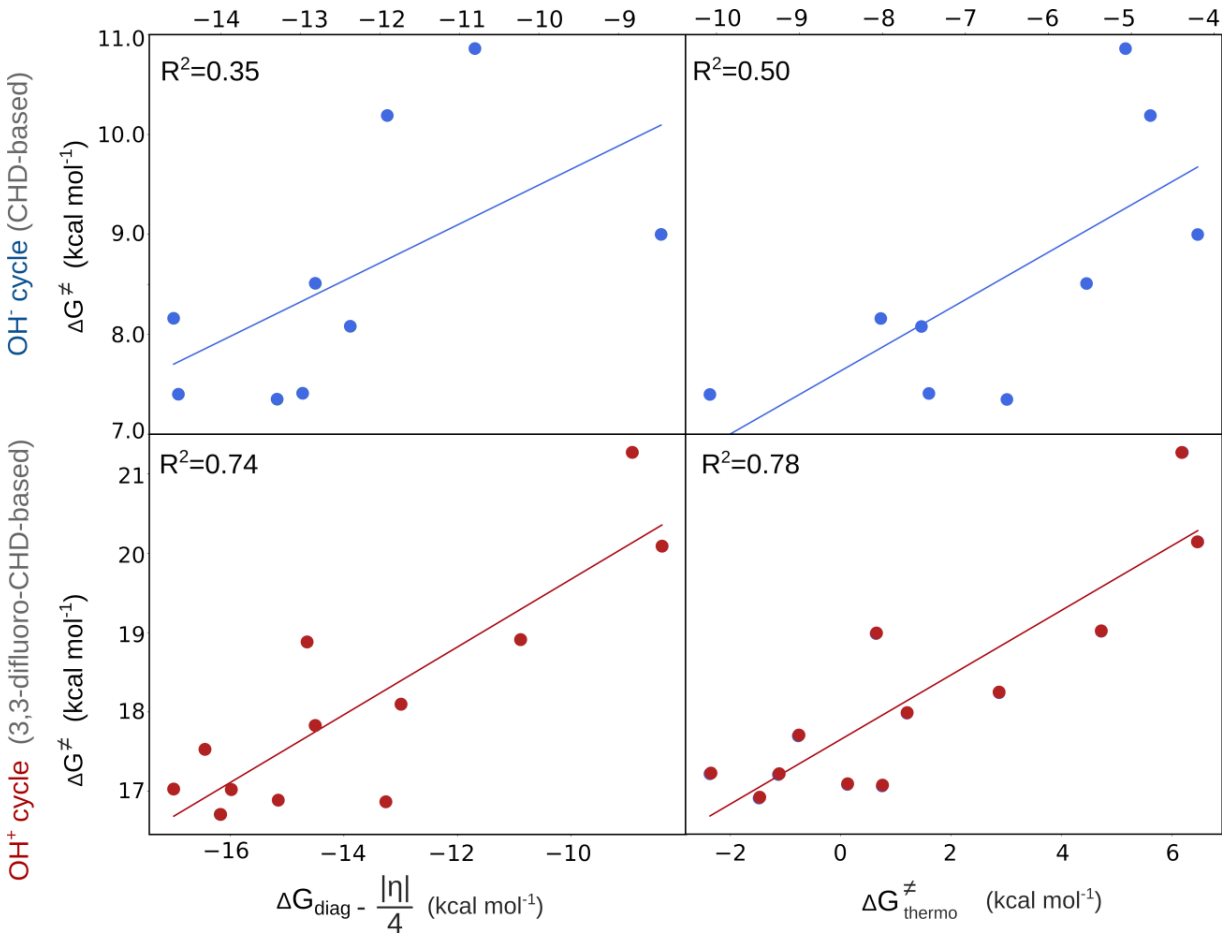

Figure S8. Performance of the three-component model based on the higher off-diagonal term; $\Delta G^{\neq}$ vs: LFER with the effect of asynchronicity; LFER together with the complete off-diagonal term (asynchronicity and frustration) for the OH^- (top) and OH^+ (bottom) set. The quality of correlations is assessed by the squared Pearson's coefficient, R^2.

Table S13. Performance of the model based on the higher off-diagonal term

X axis	slope	intercept	R^2	p-value
OH^- set (antiferromagnetic)				
$\Delta G^{\neq}_{diagonal} - \frac{\lvert\eta\rvert}{4}$	0.39	11.50	0.35	0.094
$ta\Delta G^{\neq}_{thermo}$	0.47	9.77	0.50	0.033
OH+ set (antiferromagnetic)				
$\Delta G^{\neq}_{diagonal} - \frac{\lvert\eta\rvert}{4}$	0.43	22.04	0.74	0.000
$\Delta G^{\neq}_{thermo}$	0.43	15.58	0.78	0.000

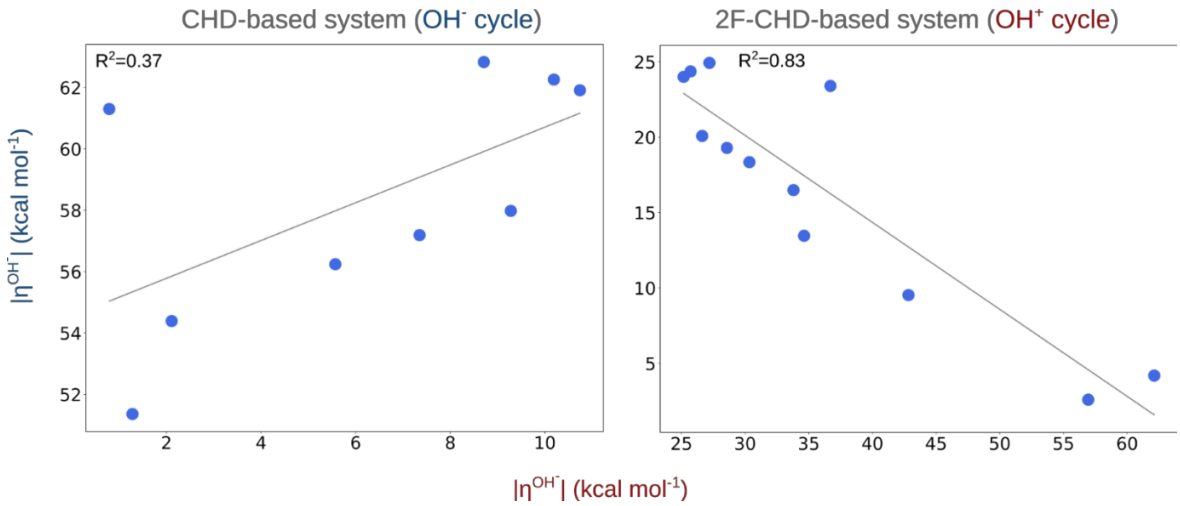

Figure S9. Correlations between |η| obtained from the OH^- and OH^+ cycle for the CHD- and 2F-CHD-based datasets.

Detailed analysis of change of electronic structure of the reactants during the reactions

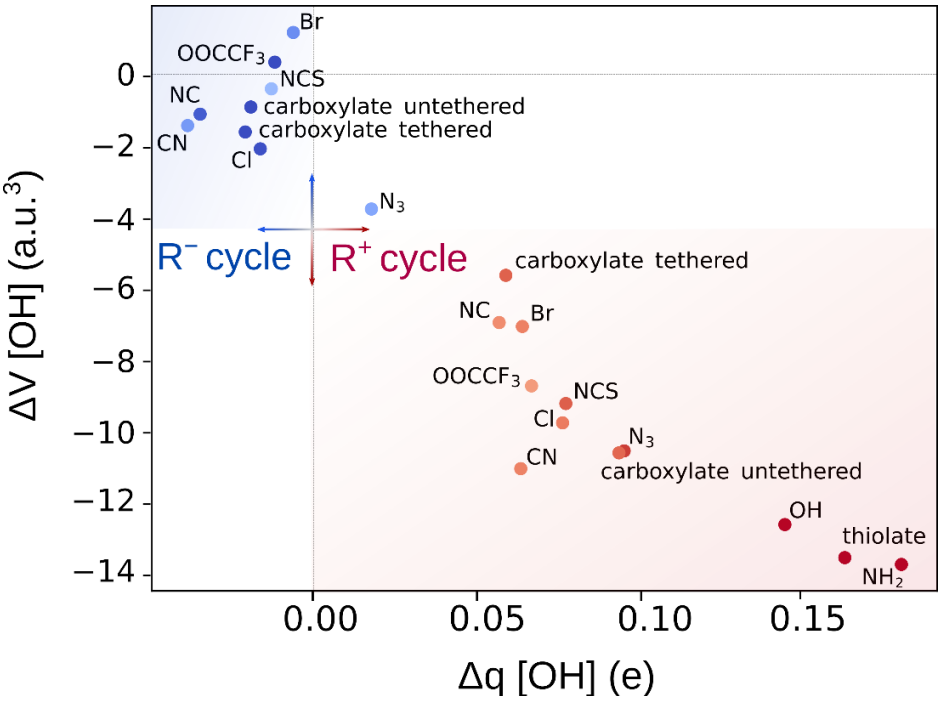

Figure S10. Characterization of the OH rebound reaction by change of volume and charge on the transferred OH group upon the RC ⟶ TS transition. The points are colored and shaded to reflect the difference of off-diagonal thermodynamic contributions to the barrier originating from the OH^- and OH^+ cycle, from blue (favored OH^-) to red (favored OH^+).

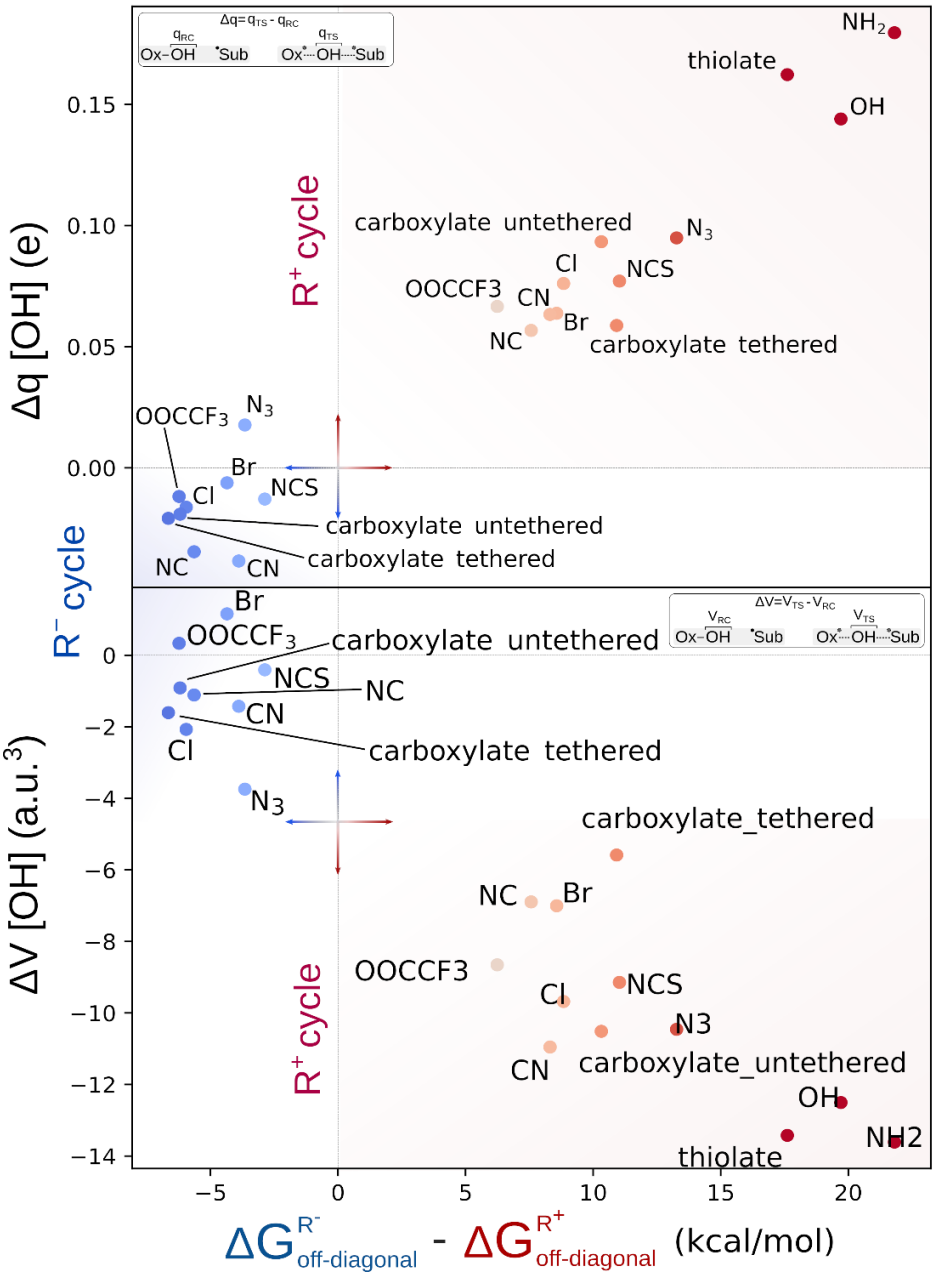

Figure S11. Correlations between the difference between the off-diagonal term obtained from the OH^- and OH^+ cycle with the change of charge (top) and volume (bottom) on the transferred OH group upon the RC ⟶ TS transition in the OH^- and OH+ cycle. The points are coloured and shaded to reflect the difference of off-diagonal thermodynamic contributions to the barrier originating from the OH^- and OH^+ cycle, from blue (favored OH^-) to red (favored OH^+).

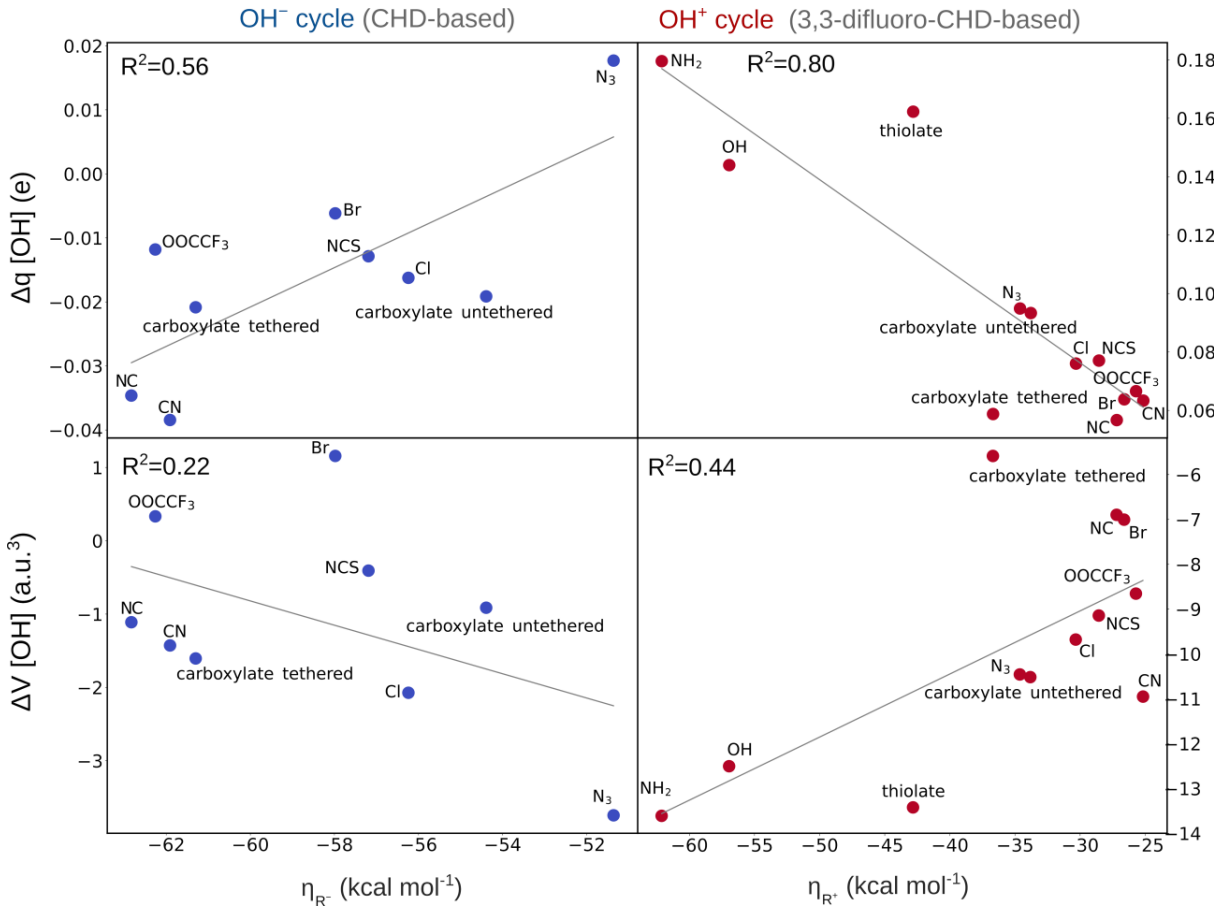

Figure S12. Correlations between η obtained from the operative thermodynamic cycle and the change of charge (top) and volume (bottom) on the transferred OH group upon the RC ⟶ TS transition in the OH− and OH+ cycle (left and right, respectively). The points are coloured to reflect the preference towards one of the thermodynamic cycles (as measured by the originating from the OH^- and OH^+ cycle) - in blue (favored OH^-) and red (favored OH^+).

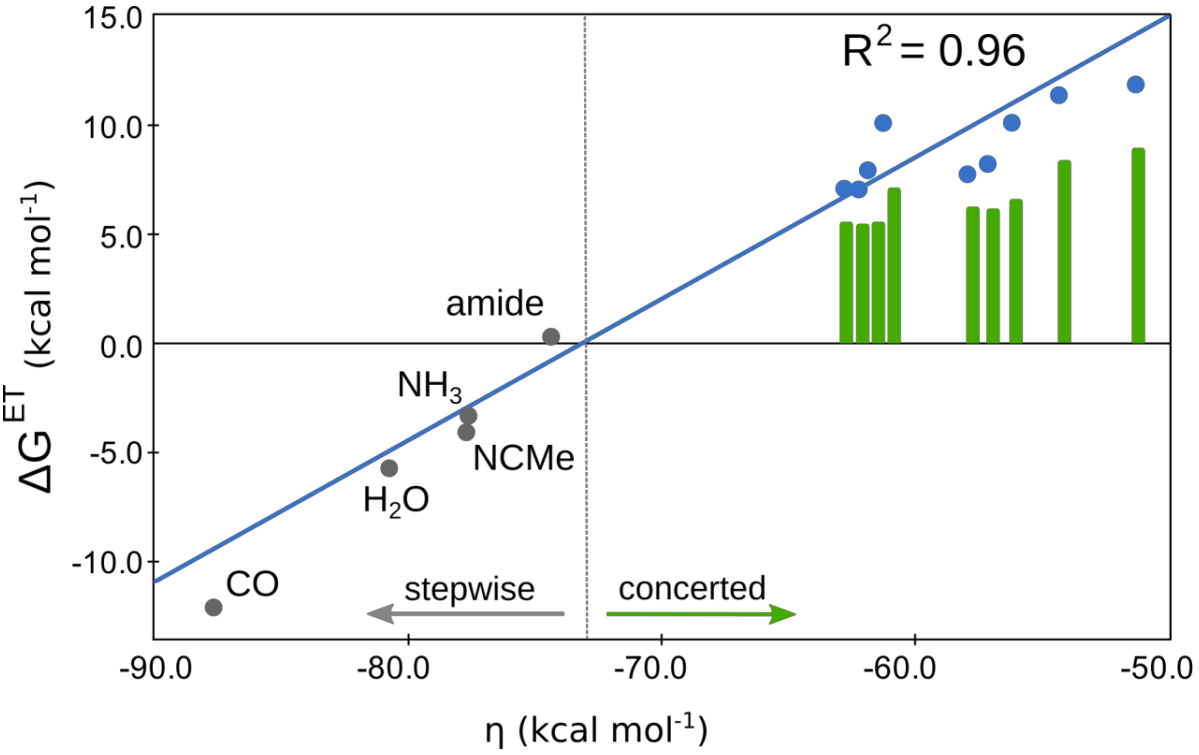

Figure S13. Correlations between η and the energy of the ET state. The green bars indicate the barrier for the concerted OH rebound, the points in grey correspond to systems featuring a neutral axial ligand (labeled in the figure). These systems were investigated only thermodynamically due to a spontaneous nature of ET leading to formation of the hydroxylated product.

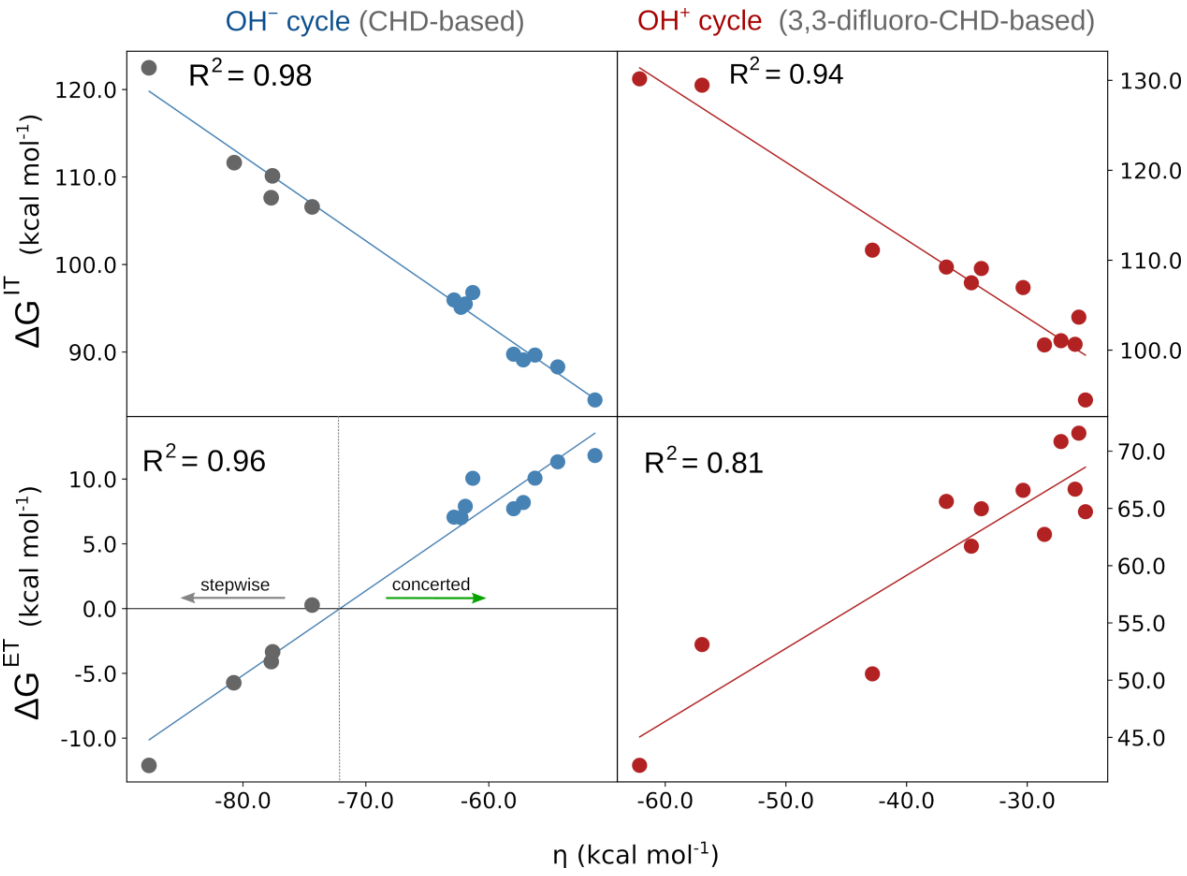

Figure S14. Correlations between η and the energy of the ET and IT states in OH^- (extended by systems undergoing a sequential, ET-driven reaction, indicated in grey) and OH^+ states.

Table S14. The composition of the orbitals of the OH rebound transition states in the (L)(TMC)Fe^{III}−OH/CHD set. All contributions > 1.0% are shown. The values are given in %.

Axial ligand	Fe - d	C• - p	C(meta) - p	Ligand - p	H(para) - s
Br	55.8	13.9	9.5 / 8.7	3.8	1.9 / 1.7
Cl	54.9	14.7	9.6 / 9.6	3.0	1.9 / 1.9
CN	55.9	14.7	9.6 / 9.0	2.1	1.9 / 1.8
NC	56.1	14.6	10.0 / 8.8	2.0	1.8 / 1.8
NCS	52.3	14.2	9.6 / 8.5	4.7 / 1.2 / 1.1 (S / N / C)	1.9 / 1.9
OH	58.6	14.9	8.8 / 8.8	< 1.0	1.6 / 1.8
NH2					
N3	50.2	15.6	9.9 / 9.8	3.0 / 2.8 (N / N)	1.2 / 1.9
OOCCF3	58.5	14.0	9.5 / 8.8	< 1.0	1.2 / 1.7
thiolate	---	---	---	---	---
carboxylate tethered	60.1	13.7	9.4 / 8.2	< 1.0	1.8 / 1.6
carboxylate untethered	60.1	13.4	8.8 / 8.4	< 1.0	1.8 / 1.6

Table S15. The composition of the orbitals of the OH rebound transition states in the (L)(TMC)Fe^{III}−OH/2F-CHD set. The component comping from the p orbital of OH group O atom is given in **bold.** Contributions > 1.0% are shown.

Axial ligand	Fe - d	C˙ - p	C(meta) - p	C(para) - p	Ligand –p	**[OH] O - p**	F - p
Br	42.5	19.3	9.9 / 9.7	1.5	8.3	**1.4**	1.4
Cl	42.9	19.9	10.1 / 10.0	1.7	5.8	**1.7**	1.5
CN	46.3	20.2	10.4 / 9.9	1.6	2.0	**1.3**	1.5
NC	46.9	12.0	10.3 / 10.0	1.6	2.2	**1.2**	1.5
NCS	38.5	18.6	9.6 / 8.9	1.6	9.4 / 3.1 (S/ N)	**1.8**	1.4
OH	46.9	18.2	9.1 / 9.1	1.9	< 1.0	**3.1**	1.4
NH2	47.7	16.8	8.7 / 8.7	2.0	< 1.0	**3.8**	1.4
N3	41.4	19.8	9.9 / 9.2	1.7	3.1 / 3.1	**1.9**	1.5
OOCCF3	46.3	19.9	10.3 / 9.6	1.7	1.4 / 1.3	**1.3**	1.5
thiolate	45.2	19.5	10.2 / 9.2	< 1.0	< 1.0	**< 0.01**	< 1.0
carboxylate tethered	45.9	20.6	10.6 / 9.9	1.6	< 0.1	**1.3**	1.5
carboxylate untethered	44.0	19.5	9.6 / 9.5	< 1.0	2.9	**2.1**	1.4

Table S16. Change of charge, Δq, on OH, (2F-)CHD• and (L)(TMC)Fe fragment in **antiferro**magnetically coupled systems.

	S=5/2 (TMC)FeIII-OH + CHD•			S=5/2 (TMC)FeIII-OH + 2F-CHD•		
ligand	**OH**	CHD•	TMC	**OH**	2F-CHD•	TMC
Br	**-0.033**	0.469	-0.437	**0.064**	0.193	-0.251
Cl	**-0.016**	0.429	-0.413	**0.076**	0.166	-0.243
CN	**-0.038**	0.445	-0.405	**0.063**	0.189	-0.254
NC	**-0.035**	0.447	-0.413	**0.057**	0.196	-0.251
NCS	**-0.021**	0.450	-0.430	**0.077**	0.183	-0.259
OH	**0.054**	0.366	-0.419	**0.144**	0.102	-0.247
NH2	**---**	---	---	**0.180**	0.081	-0.258
N3	**0.018**	0.399	-0.417	**0.095**	0.153	-0.249
OOCCF3	**-0.016**	0.274	-0.259	**0.067**	0.191	-0.259
thiolate	**---**	---	---	**0.107**	0.138	-0.159
carboxylate tethered	**-0.021**	0.456	-0.436	**0.105**	0.212	-0.317
carboxylate untethered	**-0.019**	0.464	-0.445	**0.093**	0.164	-0.257

Table S17. Change of volume, ΔV, on OH, (2F-)CHD• and (L)(TMC)Fe fragment in **antiferro**magnetically coupled system.

	S=5/2 (TMC)FeIII-OH + CHD•			S=5/2 (TMC)FeIII-OH + 2F-CHD•		
ligand	**OH**	CHD	TMC	**OH**	CHD	TMC
Br	**1.16**	-23.97	22.33	**-7.00**	-25.51	2.25
Cl	**-2.07**	-20.05	21.41	**-9.68**	-25.91	1.77
CN	**-1.43**	-21.24	21.14	**-10.95**	-20.38	7.11
NC	**-1.11**	-24.51	17.97	**-6.90**	-23.94	2.05
NCS	**-0.41**	-24.14	17.56	**-9.15**	-25.21	2.73
OH	***-8.98***	*-20.32*	*21.39*	**-12.50**	-24.60	-0.36
NH2	**---**	---	---	**-13.61**	-25.62	-1.92
N3	**-3.74**	-22.89	16.35	**-10.46**	-25.63	0.47
OOCCF3	**0.33**	-14.26	11.51	**-8.66**	-24.77	2.36
thiolate	**---**	---	---	**-13.42**	-23.16	1.26
carboxylate tethered	**-1.61**	-26.30	17.68	**-12.03**	-21.31	3.42
carboxylate untethered	**-0.91**	-22.96	20.48	**-10.51**	-22.01	4.55

Differences between the reactions with CHD and 2F-CHD

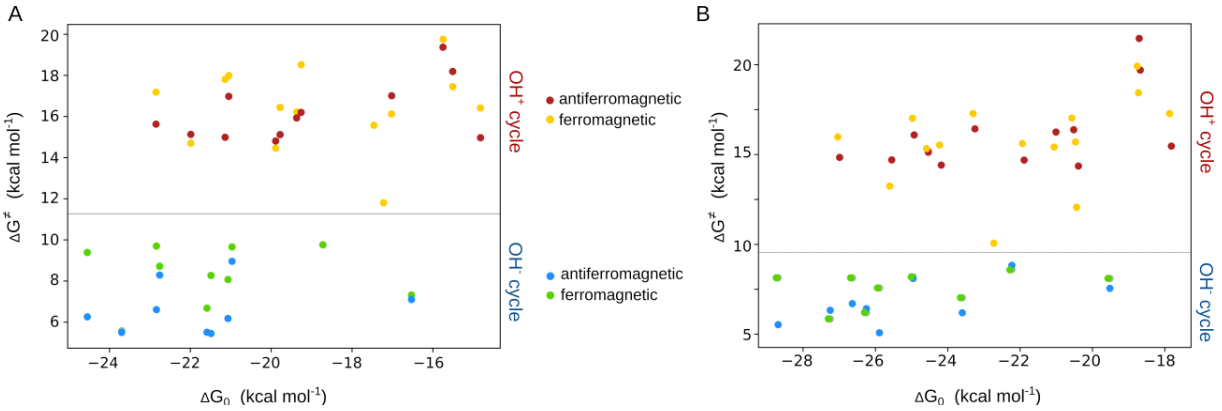

Figure S15. Barriers for the antiferro- and ferromagnetically coupled reactants in the parallel (**A**) and crossed set (**B**). The points are colored according to the dataset: blue – OH^-, antiferromagnetically coupled reactants, green – OH^-, ferromagnetically coupled reactants, red – OH^+, antiferromagnetically coupled reactants, yellow – OH^+, ferromagnetically coupled reactants

Table S18. Crucial geometric parameters for OH rebound transition states in the (L)(TMC)Fe^{III}−OH/(2F-)CHD set ('parallel', **antiferromagnetically** coupled reactants). System given in *italics* follows the OH^+ cycle.

	CHD				2F-CHD			
	C----O distance (Å)	Fe----O distance (Å)	Fe-O-C angle (deg)	Fe-O-H angle (deg)	C----O distance (Å)	Fe----O distance (Å)	Fe-O-C angle (deg)	Fe-O-H angle (deg)
Br	2.53	1.98	161.8	122.0	2.11	2.05	161.3	111.6
Cl	2.45	1.98	162.3	119.8	2.07	2.04	160.7	111.0
CN	2.49	1.98	162.2	124.1	2.13	2.01	159.4	114.7
NC	2.49	1.97	159.8	123.8	2.12	2.01	158.1	114.9
NCS	2.47	1.98	159.9	122.8	2.08	2.02	159.8	112.7
OH	*2.27*	*2.06*	*164.4*	*113.2*	1.96	2.11	160.8	107.8
NH2	---	---	---	---	1.94	2.16	168.1	97.3
N3	2.38	1.99	160.2	120.1	2.05	2.04	159.5	111.5
OOCCF3	2.54	1.96	160.4	122.4	2.09	2.01	159.7	113.0
thiolate	---	---	---	---	2.04	2.06	160.5	111.0
carboxylate tethered	2.44	1.98	159.7	120.3	2.05	2.01	157.9	113.2
carboxylate untethered	2.45	1.99	162.0	119.7	2.05	2.04	159.9	112.0

Table S19. Crucial geometric parameters for OH rebound transition states in the (L)(TMC)Fe^{III}−OH/(2F-)CHD set ('parallel', **ferromagnetically** coupled reactants). CHD-based systems given in *italics* follows the OH^+ cycle.

	CHD				2F-CHD			
	C----O distance (Å)	Fe----O distance (Å)	Fe-O-C angle (deg)	Fe-O-H angle (deg)	C----O distance (Å)	Fe----O distance (Å)	Fe-O-C angle (deg)	Fe-O-H angle (deg)
Br	2.78	1.87	173.6	115.9	2.20	1.99	168.0	107.2
Cl	2.89	1.82	177.0	119.9	2.21	1.97	168.7	105.4
CN	2.50	1.98	167.0	113.2	2.10	2.01	166.9	105.9
NC	2.57	1.90	175.9	114.4	2.15	1.99	166.9	107.0
NCS	2.59	1.89	178.1	113.9	2.15	1.98	166.6	107.4
OH	*2.27*	*2.02*	*172.7*	*106.0*	1.94	2.16	168.1	97.3
NH_2	*2.20*	*2.06*	*170.8*	*105.1*	2.03	2.05	167.8	102.4
N_3	2.63	1.87	177.5	115.4	2.13	1.99	167.0	106.0
$OOCCF_3$	2.77	1.85	172.2	117.0	2.17	1.97	167.5	107.1
thiolate	*2.27*	*2.03*	*171.4*	108.4	2.03	2.06	167.2	103.9
carboxylate tethered	2.59	1.89	171.8	114.8	2.09	1.98	167.1	105.8
carboxylate untethered	2.64	1.89	174.6	114.2	2.17	1.98	169.0	105.2

Table S20. Crucial geometric parameters for OH rebound transition states in the (L)(TMC)Fe^{III}−OH/(2F-)CHD set ('crossed', **antiferromagnetically** coupled reactants). System given in *italics* follows the OH^+ cycle.

	CHD				2F-CHD			
	C----O distance (Å)	Fe----O distance (Å)	Fe-O-C angle (deg)	Fe-O-H angle (deg)	C----O distance (Å)	Fe----O distance (Å)	Fe-O-C angle (deg)	Fe-O-H angle (deg)
Br	2.61	1.98	168.6	119.9	2.11	2.06	161.3	111.4
Cl	2.55	2.00	168.9	118.1	2.08	2.06	158.1	113.3
CN	2.49	1.99	158.6	124.5	2.13	2.03	159.0	114.3
NC	2.48	1.99	157.9	125.4	2.11	2.02	156.1	115.8
NCS	2.52	1.98	164.2	121.5	2.09	2.03	158.9	113.2
OH	*2.29*	*2.07*	*164.1*	*113.8*	1.96	2.14	160.0	108.6
NH_2	---	---	---	---	1.92	2.22	160.9	106.2
N_3	2.37	1.99	162.2	119.9	2.05	2.06	159.7	111.3
$OOCCF_3$	2.49	1.98	157.6	123.6	2.10	2.02	158.5	113.9
thiolate	---	---	---	---	2.05	2.08	161.2	110.7
carboxylate tethered	2.40	1.98	163.7	122.7	2.05	2.02	154.7	114.6
carboxylate untethered	2.46	2.00	168.4	120.6	2.05	2.06	148.6	113.5

Table S21. Crucial geometric parameters for OH rebound transition states in the (L)(TMC)Fe^{III}−OH/(2F-)CHD set ferromagnetic ('crossed', **ferromagnetically** coupled reactants).

	CHD				2F-CHD			
	C----O distance (Å)	Fe----O distance (Å)	Fe-O-C angle (deg)	Fe-O-H angle (deg)	C----O distance (Å)	Fe----O distance (Å)	Fe-O-C angle (deg)	Fe-O-H angle (deg)
Br	2.78	1.87	173.6	115.9	2.23	2.00	168.5	106.6
Cl	2.81	1.86	174.2	119.5	2.21	2.00	170.3	106.0
CN	2.40	1.97	174.3	110.8	2.10	2.01	167.5	105.4
NC	2.63	1.90	172.7	115.0	2.16	2.00	164.7	107.9
NCS	2.75	1.87	169.3	116.9	2.17	1.99	167.4	106.4
OH	2.26	2.02	172.6	106.4	2.02	2.07	166.1	103.5
NH_2	2.19	2.06	172.0	105.4	1.97	2.12	168.1	101.1
N_3	2.62	1.88	177.3	114.6	2.15	2.00	168.4	104.7
$OOCCF_3$	2.85	1.86	169.2	120.8	2.21	1.98	168.8	106.0
thiolate	2.34	2.03	171.2	110.7	2.03	2.07	166.7	104.8
carboxylate tethered	2.54	1.91	177.9	111.6	2.11	1.99	153.7	106.8
carboxylate untethered	2.63	1.88	177.5	115.0	2.16	2.01	152.3	105.8

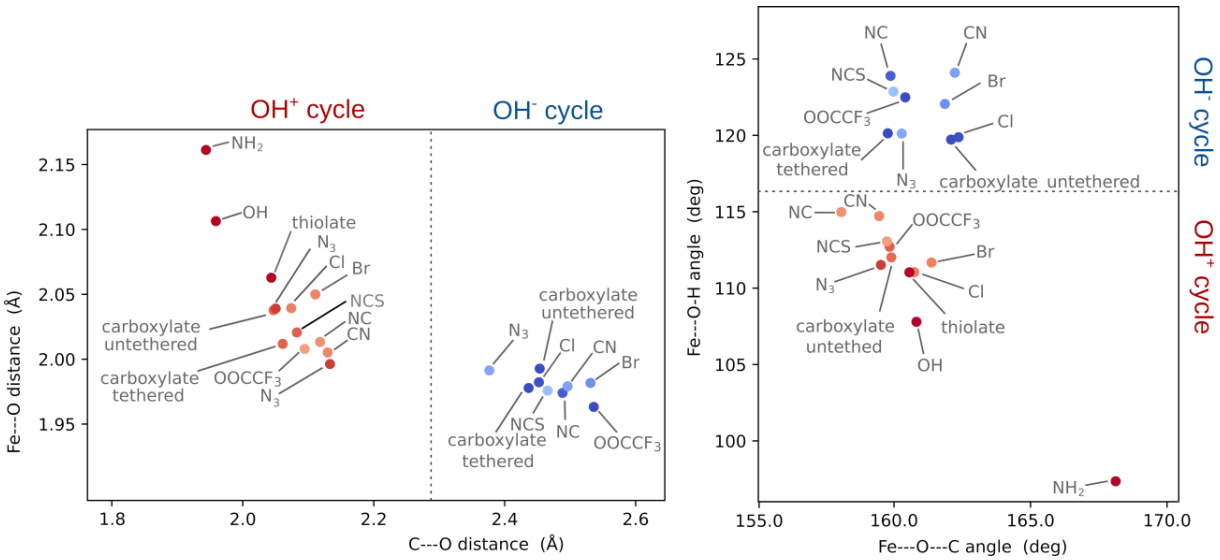

Figure S16. Crucial distances (right) and angles (left) for the CHD and 2F-CHD transition states ('parallel' set, antiferromagnetically coupled reactants). The points are colored and shaded to reflect the difference of off-diagonal thermodynamic contributions to the barrier originating from the OH^- and OH^+ cycle, from blue (favored OH^-) to red (favored OH^+).

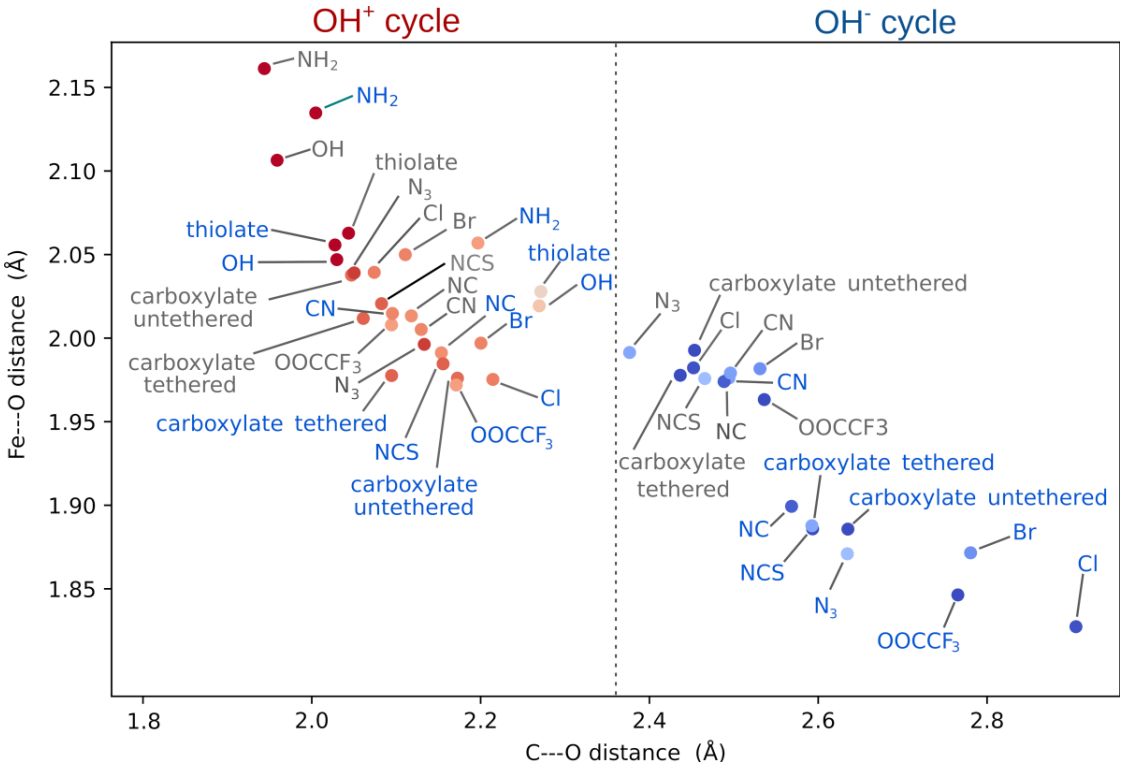

Figure S17. Crucial distances for the CHD and 2F-CHD transition states ('parallel' set). Antiferromagnetically coupled TSs are labeled with grey, ferromagnetically coupled ones with blue. The points are colored and shaded to reflect the difference of off-diagonal thermodynamic contributions to the barrier originating from the OH^- and OH^+ cycle, from blue (favored OH^-) to red (favored OH^+).

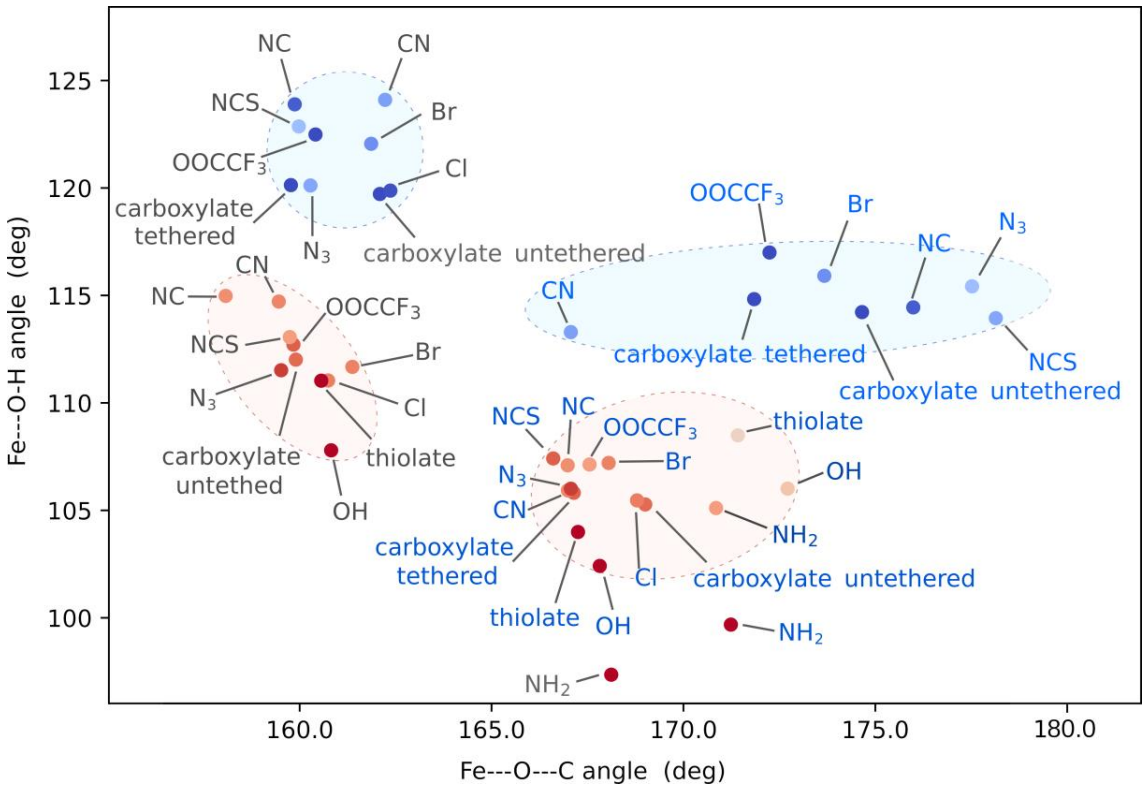

Figure S18. Crucial angles for the CHD and 2F-CHD transition states ('parallel' set). Antiferromagnetically coupled TSs are labeled with grey, ferromagnetically coupled ones with blue. The points are colored and shaded to reflect the difference of off-diagonal thermodynamic contributions to the barrier originating from the OH^- and OH^+ cycle, from blue (favored OH^-) to red (favored OH^+).

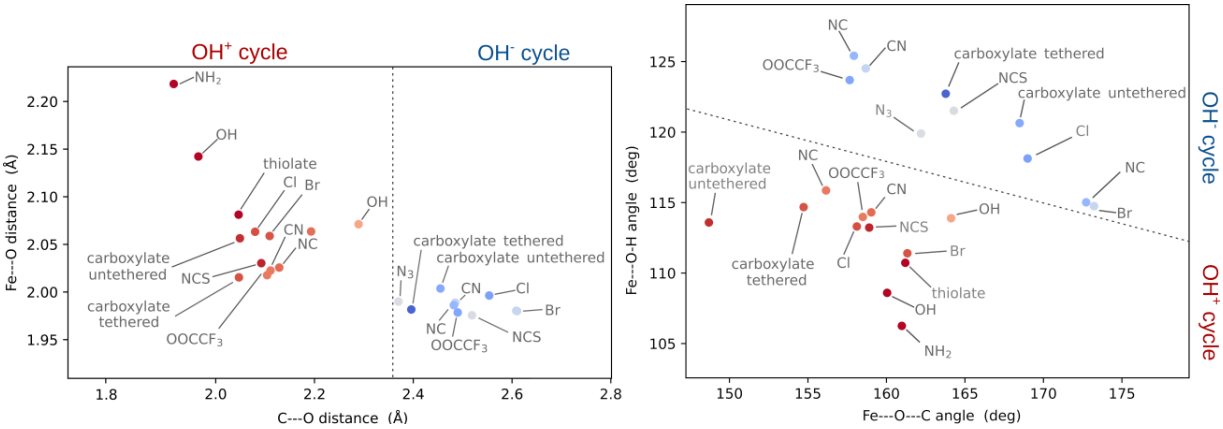

Figure S19. Crucial distances (right) and angles (left) for the CHD and 2F-CHD transition states ('crossed' set, antiferromagnetically coupled reactants). The points are colored and shaded to reflect the difference of off-diagonal thermodynamic contributions to the barrier originating from the OH^- and OH^+ cycle, from blue (favored OH^-) to red (favored OH^+).

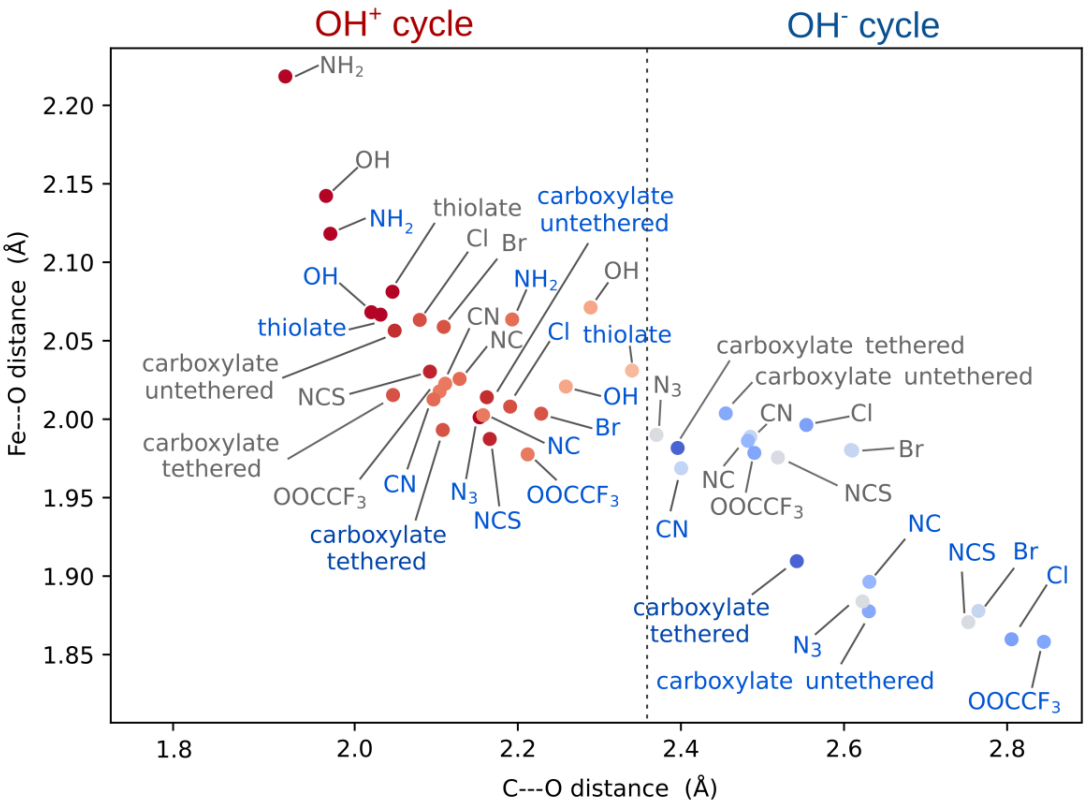

Figure S20. Crucial distances for the CHD and 2F-CHD transition states ('crossed' set). Antiferromagnetically coupled TSs are labeled with grey, ferromagnetically coupled ones with blue. The points are colored and shaded to reflect the difference of off-diagonal thermodynamic contributions to the barrier originating from the OH^- and OH^+ cycle, from blue (favored OH^-) to red (favored OH^+).

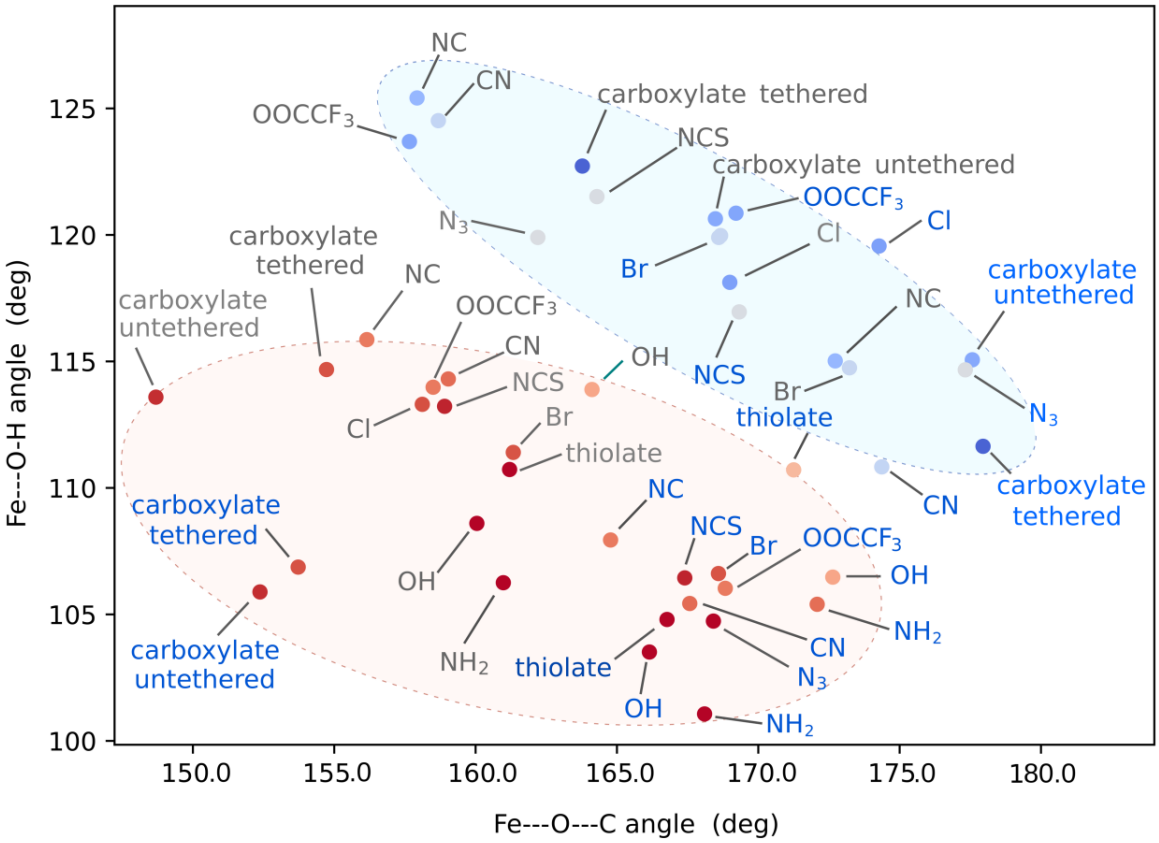

Figure S21. Crucial angles for the CHD and 2F-CHD transition states ('parallel' set). Antiferromagnetically coupled TSs are labeled with grey, ferromagnetically coupled ones with blue. The points are colored and shaded to reflect the difference of off-diagonal thermodynamic contributions to the barrier originating from the OH^- and OH^+ cycle, from blue (favored OH^-) to red (favored OH^+).

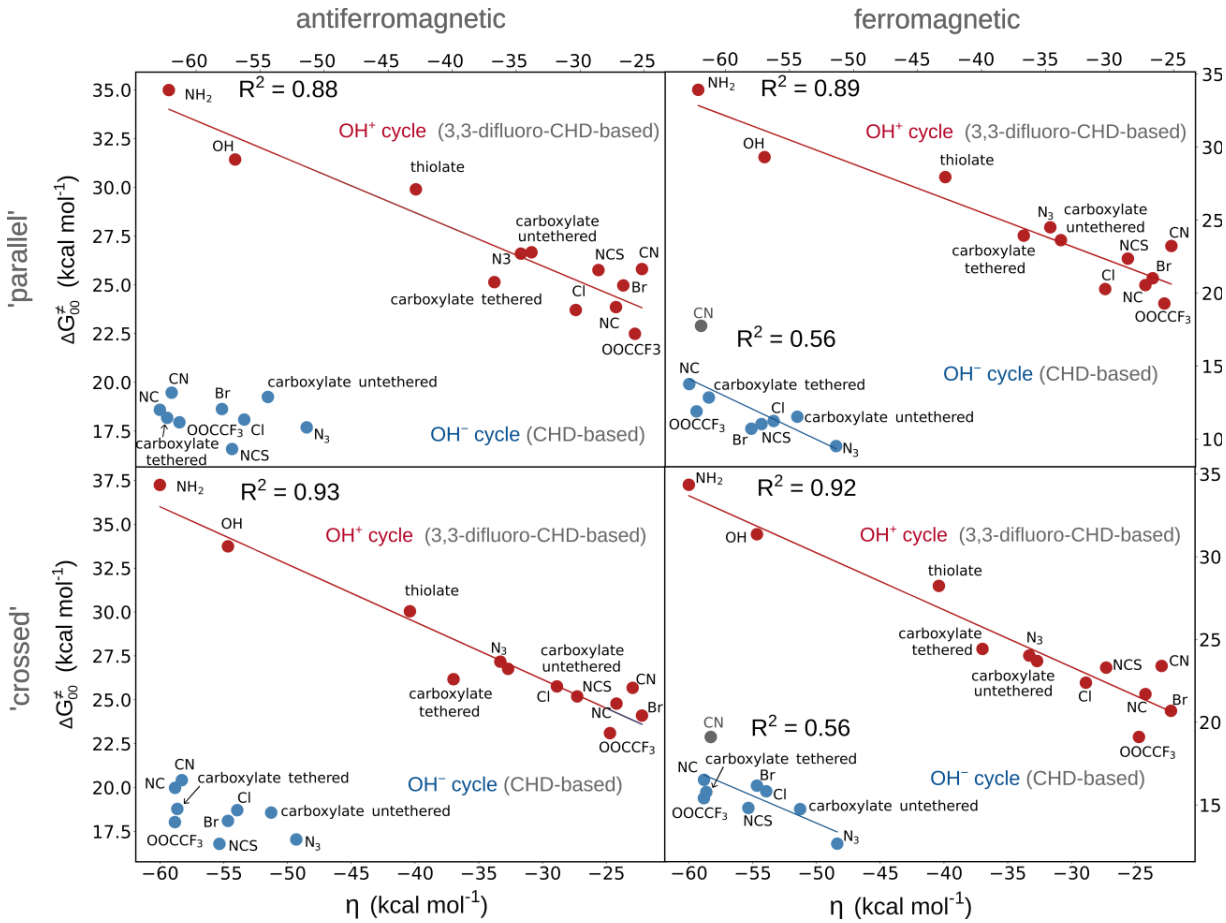

Figure S22. $\Delta G_{00}^{\neq}$ vs asynchronicity for radical transfers linked to the OH^- (blue) and OH^+ (red) thermodynamic cycles for: the parallel set – antiferromagnetically (top left) and ferromagnetically coupled reactions (top right); for the crossed set – antiferromagnetically (bottom left) and ferromagnetically coupled reactions (bottom right). For the OH^-/OH^+ sets, the η_{R^-} and η_{R^+} from eqs 3 and 4, were employed, respectively.

Characterization of the OH rebound reaction for ferromagnetically coupled reactants

The description of the OH group transfer is not affected by the spin state of $Fe^{III}OH$: the ferromagnetically coupled pairs of reactants in reactions following the OH^- or OH^+ cycle feature respectively a negative and positive change of charge on OH in going from RC to TS. The change of volume of OH also follows the same pattern in space of ferromagnetically and antiferromagnetically coupled systems, that is only a modest change in case of reactions linked to OH- cycle-following reaction, and a noticeable decrease of volume for the OH^+ counterpart, only the absolute changes in the ferromagnetic space are more shifted towards positive values.

The origin of the shift was rationalized by a separate inspection of the transition state structures for OH rebound and $Fe^{III}OH$ complexes. It turns out that the absolute volume of the OH group depends solely on the mechanism for the reaction, and not on spin state of the $Fe^{III}OH$ complex (and stays within the range of 101-112 $a.u.^3$ for OH^--flavored reactions and 97-101 $a.u.^3$ for OH^+ cycle-affected reactions). On the other hand, the spin state of $Fe^{III}OH$ affects the volume of the OH group in the reactant complex– the S=3/2 (L)(TMC)Fe^{III}–OH complexes feature a more compact OH group than the S=5/2 counterparts. Therefore, the increase of volume in case of OH^- cycle following reaction is more pronounced in the ferromagnetically coupled set and, in the same fashion, the decrease of volume in case of OH^+ is less marked, which can be possibly attributed to an unoccupied dz^2 orbital in the intermediate spin complexes.

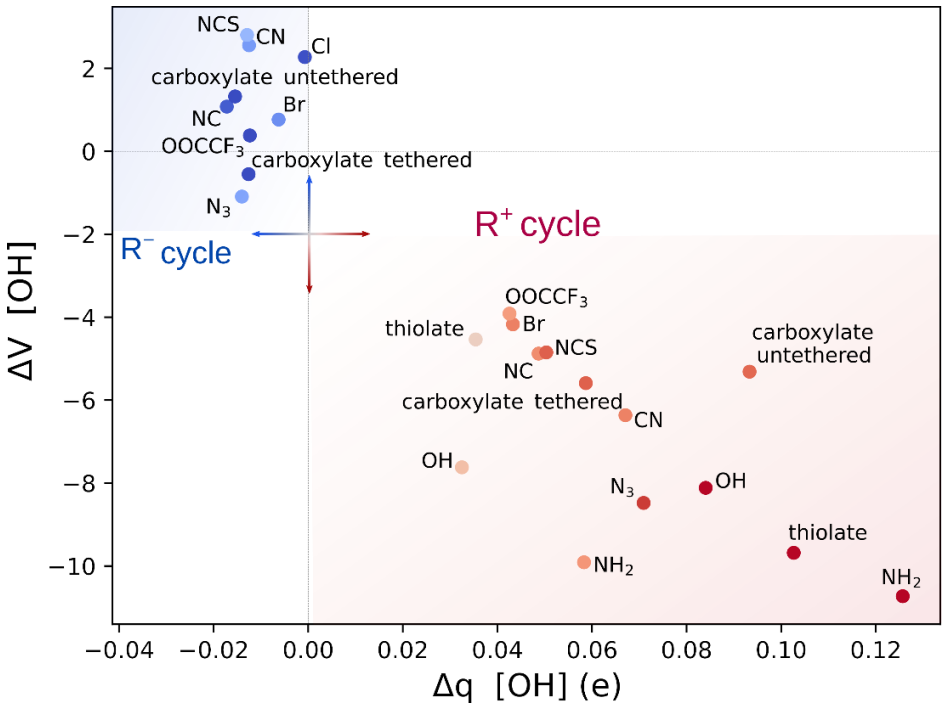

Figure S23. Characterization of the OH rebound reaction for ferromagnetically coupled reactants by change of volume and charge on the transferred OH group upon the RC ⟶ TS transition. The points are colored and shaded to reflect the difference of off-diagonal thermodynamic contributions to the barrier $\Delta G^{\neq}_{\text{off-diagonal}}$ originating from the OH^- and OH^+ cycle, from blue (favored OH^-) to red (favored OH^+).

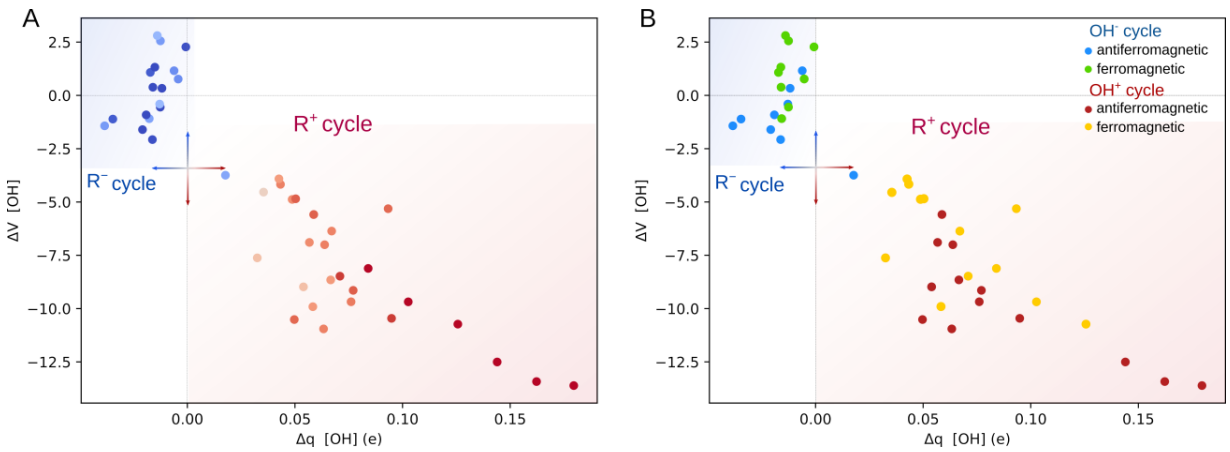

Figure S24. Characterization of the OH rebound reaction for all investigated systems by change of volume and charge on the transferred OH group upon the RC ⟶ TS transition. The points are colored and shaded: to reflect the difference of off-diagonal thermodynamic contributions to the barrier originating from the OH^- and OH^+ cycle, from blue (favored OH^-) to red (favored OH^+) (**A**) according to the system – (L)(TMC)Fe^{III}–OH with CHD$^\bullet$ antiferromagnetically coupled (blue), (L)(TMC)Fe^{III}–OH with CHD$^\bullet$ ferromagnetically coupled (green), (TMC)Fe^{III}–OH with 2F-CHD$^\bullet$ antiferromagnetically coupled (red), TMC)Fe^{III}–OH with 2F-CHD$^\bullet$ ferromagnetically coupled (orange) (**B**).

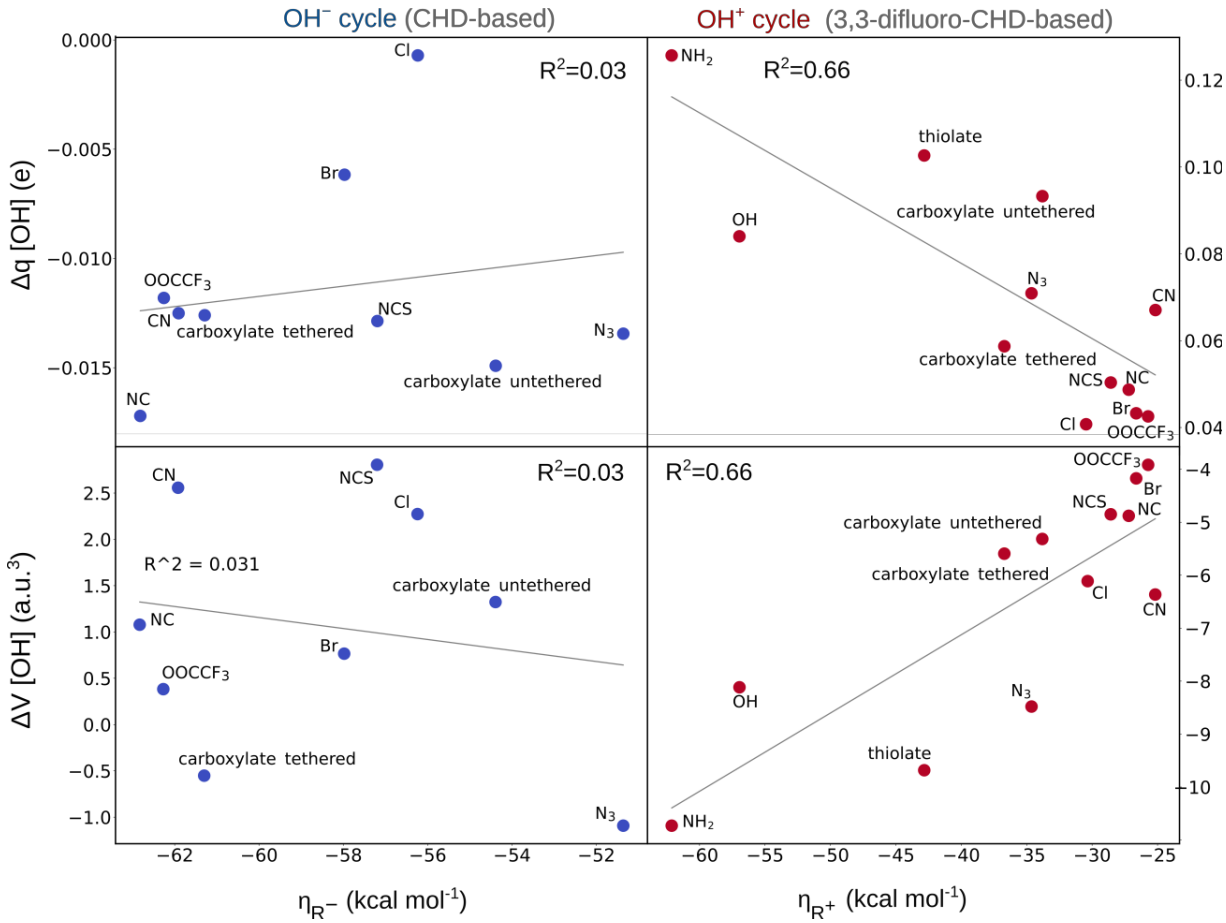

Figure S25. Correlations between η obtained from the operative thermodynamic cycle and the change of charge (top) and volume (bottom) on the transferred OH group upon the RC ⟶ TS transition in the OH− and OH+ cycle (left and right, respectively). The points are colored to reflect the preference towards one of the thermodynamic cycles (as measured by the $\Delta G^{\neq}_{\text{off-diagonal}}$ originating from the OH^- and OH^+ cycle) - in blue (favored OH^-) and red (favored OH^+).

Table S22. Change of charge, Δq, on OH, (2F-)CHD• and (L)(TMC)Fe fragment in **ferro**magnetically coupled systems.

	S=3/2 (TMC)FeIII-OH + CHD•			S=3/2 (TMC)FeIII-OH + 2F-CHD•		
ligand	**OH**	CHD	TMC	**OH**	CHD	TMC
Br	**-0.006**	0.106	-0.099	**0.043**	0.231	-0.274
Cl	**-0.001**	0.085	-0.082	**0.041**	0.246	-0.288
CN	**-0.013**	0.420	-0.409	**0.067**	0.220	-0.290
NC	**-0.017**	0.294	-0.273	**0.049**	0.225	-0.274
NCS	**-0.013**	0.296	-0.275	**0.050**	0.224	-0.277
OH	**0.032**	0.374	-0.406	**0.084**	0.191	-0.277
NH2	**0.058**	0.363	-0.421	**0.126**	0.129	-0.277
N3	**-0.013**	0.261	-0.248	**0.071**	0.207	-0.279
OOCCF3	**-0.012**	0.149	-0.150	**0.043**	0.228	-0.274
thiolate	**0.035**	0.386	-0.422	**0.103**	0.175	-0.279
carboxylate tethered	**-0.013**	0.333	-0.319	**0.059**	0.203	-0.263
carboxylate untethered	**-0.015**	0.301	-0.286	**0.050**	0.245	-0.297

Table S23. Change of volume, ΔV, on OH, (2F-)CHD• and (L)(TMC)Fe fragment in **ferro**magnetically coupled system.

	S=3/2 (TMC)FeIII-OH + CHD•			S=3/2 (TMC)FeIII-OH + 2F-CHD•		
ligand	**OH**	CHD	TMC	**OH**	CHD	TMC
Br	**0.77**	5.58	-9.45	**-4.17**	-23.66	18.06
Cl	**2.27**	-0.72	10.63	**-6.11**	-25.70	19.48
CN	**2.56**	25.81	-32.86	**-6.36**	-25.19	19.60
NC	**1.08**	-13.63	26.03	**-4.88**	-23.77	17.67
NCS	**2.81**	15.62	-25.12	**-4.85**	-23.10	17.17
OH	**-7.62**	-22.10	31.79	**-8.12**	-26.13	13.26
NH2	**-9.91**	-25.78	31.71	**-10.73**	-26.18	13.87
N3	**-1.09**	10.42	-25.32	**-8.48**	-23.48	15.15
OOCCF3	**0.38**	8.23	-12.51	**-3.91**	-23.67	16.57
thiolate	**-4.54**	-24.14	32.43	**-9.68**	-21.65	19.34
carboxylate tethered	**-0.55**	-15.94	24.29	**5.59**	21.39	-11.68
carboxylate untethered	**1.32**	16.86	-24.83	**-5.31**	-23.10	20.86